ARTICLES
https://doi.org/10.1038/s41590-020-0643-3
nature immunology

Check for updates

Sestrins induce natural killer function in senescent-like CD8+ T cells

Branca I. Pereira[1,14], Roel P. H. De Maeyer[1,14], Luciana P. Covre[1,2,14], Djamel Nehar-Belaid[3,14], Alessio Lanna[1,4], Sophie Ward[5], Radu Marches[3], Emma S. Chambers[1], Daniel C. O. Gomes[2], Natalie E. Riddell[1,6], Mala K. Maini[1], Vitor H. Teixeira[7], Samuel M. Janes[7], Derek W. Gilroy[8], Anis Larbi[9], Neil A. Mabbott[10], Duygu Ucar[3], George A. Kuchel[11], Sian M. Henson[12], Jessica Strid[5], Jun H. Lee[13], Jacques Banchereau[3] and Arne N. Akbar[1]✉

Aging is associated with remodeling of the immune system to enable the maintenance of life-long immunity. In the CD8+ T cell compartment, aging results in the expansion of highly differentiated cells that exhibit characteristics of cellular senescence. Here we found that CD27−CD28−CD8+ T cells lost the signaling activity of the T cell antigen receptor (TCR) and expressed a protein complex containing the agonistic natural killer (NK) receptor NKG2D and the NK adaptor molecule DAP12, which promoted cytotoxicity against cells that expressed NKG2D ligands. Immunoprecipitation and imaging cytometry indicated that the NKG2D–DAP12 complex was associated with sestrin 2. The genetic inhibition of sestrin 2 resulted in decreased expression of NKG2D and DAP12 and restored TCR signaling in senescent-like CD27−CD28−CD8+ T cells. Therefore, during aging, sestrins induce the reprogramming of non-proliferative senescent-like CD27−CD28−CD8+ T cells to acquire a broad-spectrum, innate-like killing activity.

Immunity declines during aging and this is associated with an increased incidence of infections and malignancy[1]. It is therefore essential to understand mechanisms that contribute to altered immunity in older individuals in order to identify possible therapeutic targets. Because the thymus involutes from puberty onwards, its contribution to the maintenance of the T cell pool decreases considerably during aging. Instead, antigen-specific T cells are maintained in older individuals by repeated episodes of activation and proliferation triggered by specific or cross-reactive antigenic challenge or by homeostatic cytokines[2]. This extensive proliferative activity leads ultimately to extreme functional differentiation and the development of T cell senescence associated with telomere erosion, decreased signaling through the TCR, activation of the telomere-extending enzyme telomerase and growth arrest[3–5]. Because the replicative activity of T cells is impaired as senescence develops, mechanisms other than T cell proliferation may be required to maintain optimal immune protection during aging.

Highly differentiated CD8+ T cells that lose expression of the surface receptors CD27 and CD28 (CD27−CD28−) exhibit senescent-like characteristics that include low proliferative activity, short telomeres, low telomerase activity and expression of senescence-associated cell-surface (CD57 and KLRG1) and intracellular (the MAP kinase p38 and γH2AX) molecules[4]. CD27−CD28−CD8+ T cells also upregulate receptors associated with NK cells, such as inhibitory (KLRG1 and NKG2A) and activatory proteins (NKG2C and NKG2D)[6]. Whether the acquisition of the senescent-like characteristics and the expression of NK receptors (NKRs) are linked or are controlled independently remains unclear.

Sestrins are stress-sensing proteins, induced by conditions of low glucose or oxidative stress or cellular senescence, that inhibit TCR activation and CD4+ T cell proliferation in both mice and humans[7]. Here we show that sestrins inhibit the expression of the TCR signaling molecules LAT, Zap70 and Lck in mouse and human CD8+ T cells, and concomitantly induce the expression of both inhibitory and activatory NKRs. Furthermore, sestrins regulate the association of NKG2D with the scaffold protein DAP12, which converts it into an activating receptor that can trigger the secretion of cytokines and cytotoxicity toward target cells bearing NKG2D ligands, independently of the TCR. Collectively, these data indicate that senescent-like CD8+ T cells are not a defective end-stage population. Instead, these cells, although non-proliferative, are reprogrammed during differentiation to recognize and kill through both TCR[8] as well as NKR recognition mechanisms, a process regulated by the sestrins. The repurposing of senescent-like CD8+ T cells to mediate innate-like functional activity may be crucial to mitigate against the increased burden of tumors and stromal senescent cells that accumulate in tissues during aging[9,10].

Results

Human CD8+ T_{EMRA} cells upregulate NK receptors but decrease TCR components. First, we isolated peripheral blood CD8+ T cell subsets from six healthy donors and compared the transcriptomes

[1]Division of Infection and Immunity, University College London, London, UK. [2]Núcleo de Doenças Infecciosas, Universidade Federal do Espírito Santo, Vitória, Brazil. [3]The Jackson Laboratory for Genomic Medicine, Farmington, CT, USA. [4]Nuffield Department of Medicine, University of Oxford, Oxford, UK. [5]Department of Medicine, Imperial College London, London, UK. [6]Faculty of Health & Medical Sciences, University of Surrey, Guildford, UK. [7]Lungs for Living Research Centre, UCL Respiratory, University College London, London, UK. [8]Division of Medicine, University College London, London, UK. [9]Singapore Immunology Network (SIgN), Agency for Science, Technology and Research (A*STAR), Biopolis, Singapore, Singapore. [10]Roslin Institute and Royal (Dick) School of Veterinary Studies, University of Edinburgh, Edinburgh, UK. [11]University of Connecticut Center on Aging, University of Connecticut, Farmington, CT, USA. [12]William Harvey Research Institute, Barts and The London School of Medicine and Dentistry, Queen Mary University of London, London, UK. [13]Department of Molecular & Integrative Physiology, University of Michigan, Ann Arbor, MI, USA. [14]These authors contributed equally: Branca I. Pereira, Roel P. H. De Maeyer, Luciana P. Covre, Djamel Nehar-Belaid. ✉e-mail: a.akbar@ucl.ac.uk

of CD27$^+$CD45RA$^-$CD8$^+$ central memory T cells (T_{CM} cells), CD27$^-$CD45RA$^-$CD8$^+$ effector memory T cells (T_{EM} cells) and CD27$^-$CD45RA$^+$CD8$^+$ terminal effector memory T cells (T_{EMRA} cells) relative to the CD27$^+$CD45RA$^+$CD8$^+$ naive T cells (T_N cells) using Affymetrix U133 plus 2.0 microarrays (Fig. 1a and Extended Data Fig. 1a). Differentially expressed genes in these CD8$^+$ T cell subsets were identified on the basis of a minimum of a twofold change ($P < 0.05$, false-discovery rate (FDR) for multiple comparisons < 0.05%; Supplementary Table 1). Hierarchical clustering of genes associated with effector cell function indicated a transcriptional signature that distinguished T_{EMRA} cells from T_N cells (Fig. 1b,c). Genes that are involved in costimulation (*Cd28* and *Cd27*), TCR signaling (*Trac*, *Cd3e*, *Cd3g*, *Lck*, *Lat* and *Plcg1)* and proliferation and cell cycle control (*Ccne1* and *Ccnd3*) were downregulated in T_{EMRA} cells compared to T_N cells (Fig. 1b,c). Compared to CD8$^+$ T_N cells, CD8$^+$ T_{EMRA} cells upregulated the transcription factor-encoding genes *Zeb2* (fold change: 10.75, $P < 0.0001$) and *Zbtb16* (encodes the zinc finger protein PLZF, fold change: 6.48, $P < 0.0001$; Fig. 1b and Supplementary Table 2) which are known to regulate terminal differentiation of memory T cells[11] and the development of innate-like features in T cells in mice[12,13]. Expression of *Zbtb16* was also increased in T_{CM} cells and T_{EM} cells compared to its expression T_N cells (7.7-fold and 4.8-fold, respectively; Supplementary Table 2). T_{EMRA} cells showed upregulation of genes that encode NKRs (including the *Kir* family members, *Nkg2a/c* and *Klrg1*), innate signaling adaptors (*Tyrobp*, which encodes DAP12) and molecules involved in cytotoxicity (*Gzma/b*, *Prf*, *Fasl*, *Itgav* and *Itgb1*)[14]. T_{EMRA} cells also showed upregulated expression of genes that encode chemokine receptors associated with the migration of NK cells into tissues (*Cx3cr1*, *S1pr5* and *Cmklr1*)[15], which indicates that the differentiation of CD8$^+$ T cells from T_N cells into T_{EMRA} cells was associated with a transcriptional program that promoted cytotoxic effector functions at the expense of proliferative potential and suggests that highly differentiated CD8$^+$ T cells may express effector functions independent of the TCR.

Flow cytometric analysis indicated that the expression of NKRs on non-NK cells was elevated on CD3$^+$CD27$^-$CD45RA$^+$CD8$^+$ T_{EMRA} cells (Fig. 1d and Extended Data Fig. 1a) in peripheral blood mononuclear cells (PBMCs) that were isolated from a separate cohort of healthy donors ($n = 22$; median age, 52 y; range, 25–83 y). The repertoire of NKRs expressed on CD8$^+$ T_{EMRA} cells was diverse and included both activating (NKG2D, NKG2C and KIR2DS) and inhibitory (NKG2A, KIR2DL/KIR3DL and CD244) receptors, as well as the maturation markers KLRG1 and CD57 (Fig. 1d and Extended Data Fig. 1b). Expression of CD28 and CD27 is sequentially lost on CD8$^+$ T cells as they transition from CD27$^+$CD28$^+$ CD8$^+$ T_N cells to CD27$^+$CD28$^-$ intermediate CD8$^+$ T cells and to terminal, or senescent-like, CD27$^-$CD28$^-$ CD8$^+$ T cells[16,17]. To analyze the expression of the TCR signaling machinery in CD8$^+$ T_{EMRA} cells, we isolated CD8$^+$ T cell subsets by their relative expression of CD27 and CD28, as the use of CD27 and CD28 as markers enabled the isolation of more cells for functional analyses. The CD27$^-$CD28$^-$CD8$^+$ T cell subset contained the T_{EMRA} subset and T_{EM} subset (Extended Data Fig. 1c) and had increased expression of NKRs compared to CD27$^+$CD28$^+$CD8$^+$ T_N cells (Extended Data Fig. 2a). Senescent-like CD8$^+$ T cells, identified either as CD27$^-$CD28$^-$ (refs. [18,19]) or as CD27$^-$CD45RA$^+$ (ref. [20]) increase in both number and proportion during aging and exhibit markers of senescence[4,5,7,20]. Immunoblots showed a notable downregulation of Lck, LAT and PLC-γ1, but upregulation of Zap70 in CD27$^-$CD28$^-$CD8$^+$ T cells compared to CD8$^+$ T_N cells (Fig. 1e). CD27$^-$CD28$^-$CD4$^+$ T cells also acquired cell-surface expression of NKRs (including KLRG1, NKG2C and NKG2D), but to a lesser degree than did CD27$^-$CD28$^-$CD8$^+$ T cells (Extended Data Fig. 2b). Together, these findings indicated the increased expression of NKRs on CD8$^+$ T cells with characteristics of terminal differentiation and senescence.

Individual T_{EMRA} CD8$^+$ T cells are senescent and express NK receptors and cytotoxic molecules. To investigate whether NKRs, cytotoxicity-related molecules and senescence markers were expressed on individual CD8$^+$ T_{EMRA} cells, we used single-cell RNA sequencing (scRNA-seq) to investigate the transcriptomes of ~62,000 CD8$^+$ T cells isolated from six healthy older donors (72–88 y). CD8$^+$IL-7R$^+$ and CD8$^+$IL-7R$^-$ T cells were sorted from each donor resulting in 12 samples (Extended Data Fig. 3a). Sorts yielded an average of 6,199 CD8$^+$IL-7R$^+$ cells (s.d. 1,582) and 4,192 CD8$^+$IL-7R$^-$ cells (s.d. 1,269) per donor, with an average of 1,043 and 1,011 genes per cell, respectively (Extended Data Fig. 3b,c). After discarding hybrid transcriptomes (multiplets) using Scrublet (Methods), raw data from the 12 samples (6 of CD8$^+$IL-7R$^+$ and 6 of CD8$^+$IL-7R$^-$ T cells) were combined. scRNA-seq profiles that passed the quality control (Extended Data Fig. 3d) were then corrected for technical batch effects (for example, 10× Genomics run) using the BBKNN algorithm. Unbiased clustering followed by a two-dimensional uniform manifold approximation and projection (UMAP) on the corrected data identified 13 distinct clusters (Fig. 2a). Cluster assignments were independent of batch (Extended Data Fig. 3e) and donor (Extended Data Fig. 3f) effects. The CD8$^+$IL-7R$^+$ and CD8$^+$IL-7R$^+$ cell groups were found to be associated with distinct sets of clusters (Fig. 2b). The number of cells within each cluster varied from 915 to 9,263 (Extended Data Fig. 3g) and their expression of *Il7r* mRNA was confirmed (Extended Data Fig. 4a). We assigned clusters to cell types on the basis of differential anlysis that compared expression values among cells from a given cluster to all other cells (Supplementary Table 3). All clusters expressed transcripts for *Cd3e* and *Cd8*, but not *Cd4* (Fig. 2c). We were able to identify clusters of T_N cells (expressing *Cd27*, *Ccr7*, *Sell* or *Cd28*) and T_{EMRA} cells (expressing *Klrg1*, *Prf1* or *Gzmb*) (Fig. 2c). On the basis of this expression profile, clusters C0, C4 and C8 were defined as CD8$^+$ T_N cells, and clusters C1, C2 and C6 were defined as CD8$^+$ T_{EMRA} cells (Fig. 3a). A second round of clustering performed on these six clusters confirmed the distinct transcriptomic profiles of

Fig. 1 | Transcriptional signature of human CD8$^+$ T cell subsets. a, Representative image of CD8$^+$ T cells gated on CD27$^+$CD45RA$^+$ T_N cells, CD27$^+$CD45RA$^-$ T_{CM} cells, CD27$^-$CD45RA$^-$ T_{EM} cells and CD27$^-$CD45RA$^+$ T_{EMRA} cells isolated from PBMCs from six healthy donors. Numbers in gates represent percentages of cells in each subset from a representative donor. Similar results were obtained in other experiments. **b**, Heat map of gene expression from Affymetrix U133 plus 2.0 microarrays of sorted T_N and T_{EMRA} CD8$^+$ T cell subsets, showing downregulated genes in yellow and upregulated genes in blue. **c**, The relative $\log_{10}$(fold change) of differentially expressed genes of interest (that encode the proteins shown) in T_{CM}, T_{EM} and T_{EMRA} CD8$^+$ T cell subsets as compared to T_N CD8$^+$ T cells. The list of genes of interest is shown in Supplementary Table 2 and the complete list of differentially expressed genes from the whole-transcriptome analysis (≥ 2-fold change, $P < 0.05$, FDR < 0.05%) is available in Supplementary Table 1. **d**, NKR expression on T_N, T_{CM}, T_{EM} and T_{EMRA} CD8$^+$ T cells, as assessed by flow cytometry on PBMCs from 22 healthy donors (median age, 52 y; range 25–83 y). **e**, Representative immunoblots of proximal TCR components Lck, PLCγ1, LAT and Zap70 on CD27$^+$CD28$^+$, CD27$^+$CD28$^-$ and CD27$^-$CD28$^-$ CD8$^+$ T cells freshly isolated from PBMCs using magnetic activated cell sorting (MACS). Similar data were obtained in four independent experiments. Summary data ($n = 4$) of Lck, Zap70, PLCγ1 and LAT expression normalized to the loading control (GAPDH) and presented relative to the basal expression in CD27$^+$28$^+$CD8$^+$ cells set to 1. **d**,**e**, Two-way analysis of variance (ANOVA) with Dunnett's post-test correction (**d**) and one-way ANOVA with Tukey's correction (**e**) (*$P < 0.05$, **$P < 0.01$, ***$P < 0.001$, ****$P < 0.0001$).

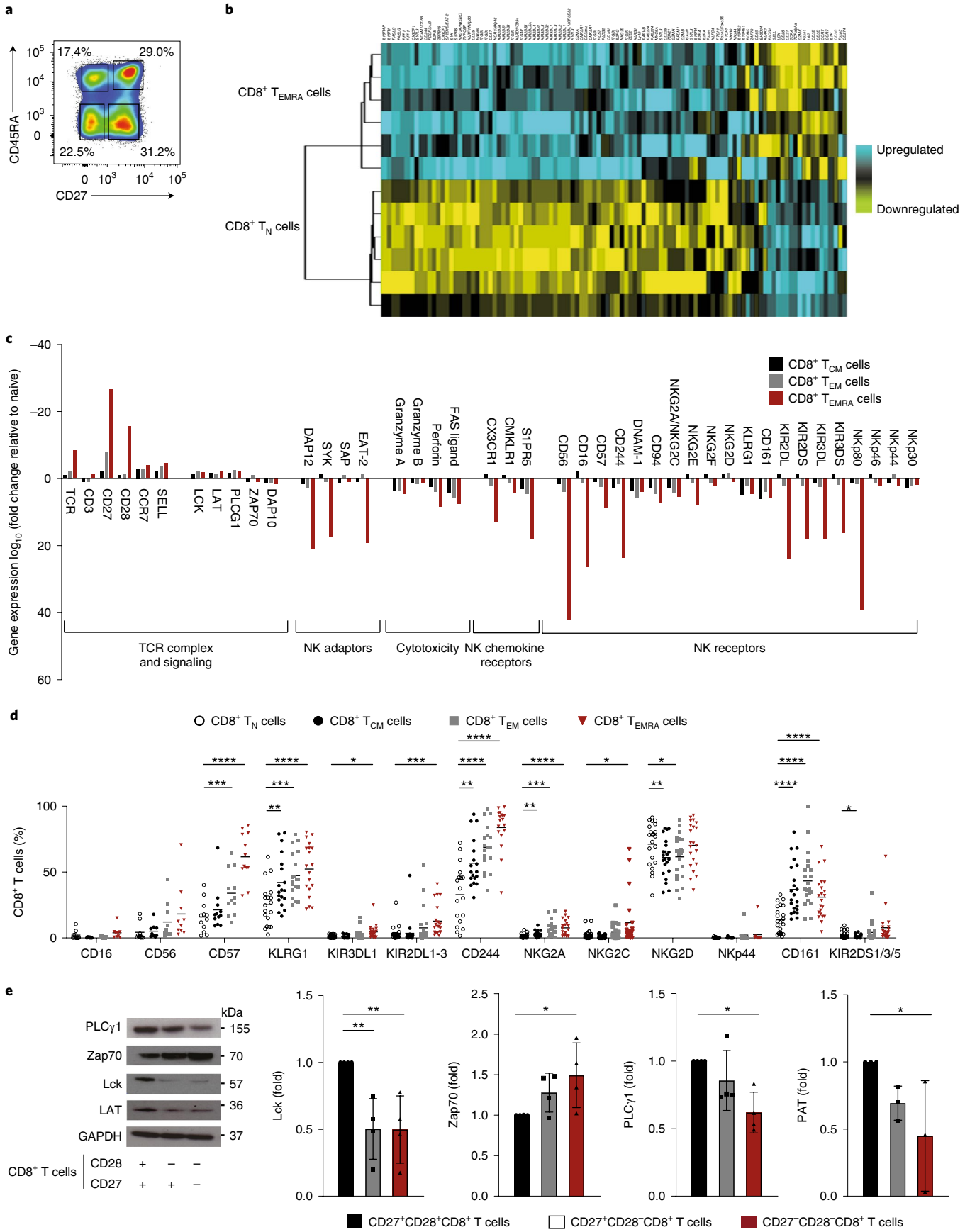
a
17.4%
29.0%
22.5%
31.2%
CD45RA
CD27
b
CD8+ TEMRA cells
CD8+ TN cells
Upregulated
Downregulated
c
Gene expression log10 (fold change relative to naive)
CD8+ TCM cells
CD8+ TEM cells
CD8+ TEMRA cells
TCR
CD3
CD27
CD28
CCR7
SELL
LCK
LAT
PLCG1
ZAP70
DAP10
DAP12
SYK
SAP
EAT-2
Granzyme A
Granzyme B
Perforin
FAS ligand
CX3CR1
CMKLR1
S1PR5
CD56
CD16
CD57
CD244
DNAM-1
CD94
NKG2A/NKG2C
NKG2E
NKG2F
NKG2D
KLRG1
CD161
KIR2DL
KIR2DS
KIR3DL
KIR3DS
NKp80
NKp46
NKp44
NKp30
TCR complex and signaling
NK adaptors
Cytotoxicity
NK chemokine receptors
NK receptors
d
CD8+ TN cells
CD8+ TCM cells
CD8+ TEM cells
CD8+ TEMRA cells
CD8+ T cells (%)
CD16
CD56
CD57
KLRG1
KIR3DL1
KIR2DL1-3
CD244
NKG2A
NKG2C
NKG2D
NKp44
CD161
KIR2DS1/3/5
e
kDa
PLCγ1
155
Zap70
70
Lck
57
LAT
36
GAPDH
37
CD8+ T cells
CD28
CD27
Lck (fold)
Zap70 (fold)
PLCγ1 (fold)
PAT (fold)
CD27+CD28+CD8+ T cells
CD27+CD28−CD8+ T cells
CD27−CD28−CD8+ T cells

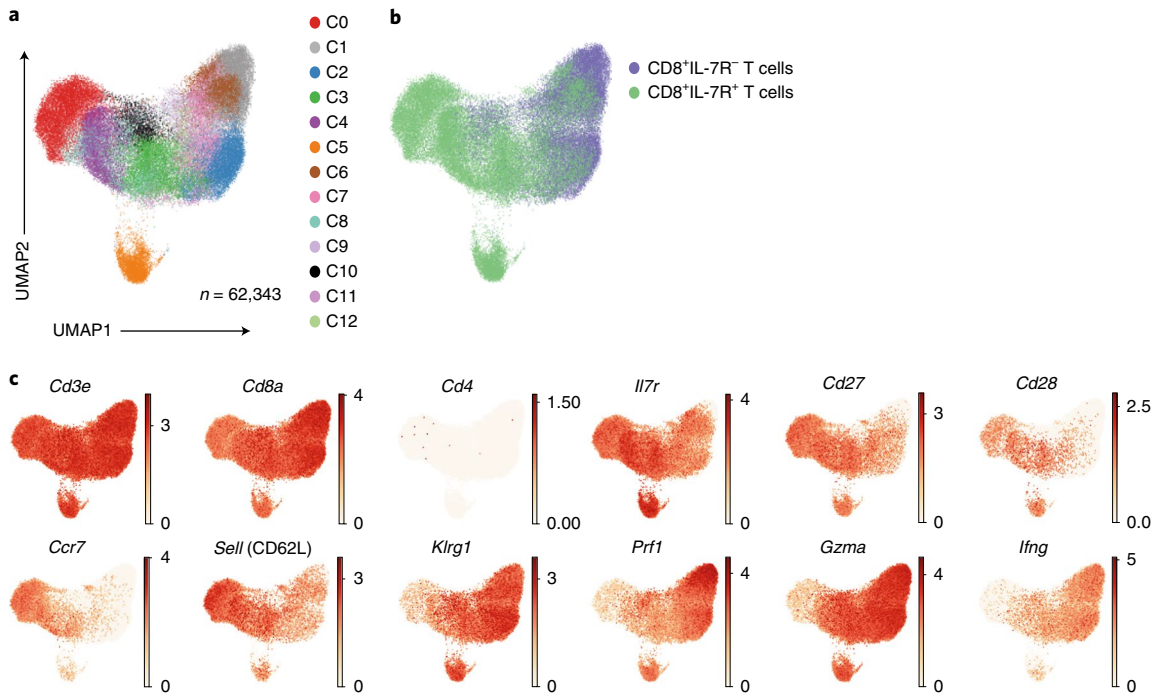

Fig. 2 | Single-cell RNA sequencing of T_N and T_{EMRA} CD8$^+$ T cells. a, UMAP visualization, with clusters demarcated by colors that identify 13 CD8$^+$ T cell clusters (C0 to C12) from RNA-seq analysis of single-cell sorted IL-7R$^+$CD8$^+$ (n = 37,192 single cells) and IL-7R$^-$CD8$^+$ (n = 25,151 single cells) T cells from six healthy older donors. **b**, UMAP plot of data from **a**, pseudocolored to show clustering of IL-7R$^+$ (in green) and IL-7R$^-$ (in purple) CD8$^+$ T cells, as identified during sorting. **c**, UMAP plot of data from **a**, representing expression values of selected individual genes. Scales show low expression (yellow) to high expression (red). Other aliases or CD numbers of proteins encoded by the listed genes are shown in brackets.

the CD8$^+$ T_N and CD8$^+$ T_{EMRA} compartments (Fig. 3b, Extended Data Fig. 4b) and confirmed the enrichment of the CD8$^+$$T_{EMRA}$ compartment within the CD8$^+$IL-7R$^-$ cells (Extended Data Fig. 4c). CD8$^+$ T_N cells were characterized by the expression of *Cd27*, *Cd28*, *Ccr7* and *Sell*, whereas CD8$^+$ T_{EMRA} cells showed an upregulation of *Klrg1*, *Prf1* or *Gzmb* relative to the clusters of CD8$^+$ T_N cells (Extended Data Fig. 4d).

The expression levels of 15 NK-associated genes, including *Fcgr3a* (which encodes the Fcγ receptor CD16) and the NK-related receptor genes *Fcrl6*, *Klrc1 and -2*, *Klrg1* and *Tyrobp* (Fig. 3c) were used to define an 'NK score'. This confirmed that CD8$^+$ T_{EMRA} cells become NK-like compared to CD8$^+$ T_N cells (Fig. 3d and Supplementary Table 4). In a similar manner, we used the expression of senescence-related genes, such as *B3gat1* (which encodes the enzyme that creates the CD57 epitope), the cell cycle regulators *Cdkn1a* and *Cdkn2a*, and sMAC components such as *Sesn2* and *Mapk1* to create a 'senescence score' to determine whether CD8$^+$ T_{EMRA} cells were senescent compared to CD8$^+$ T_N cells (Fig. 3e,f and Supplementary Table 4). Although the expression of Lck, PLC-γ1 and LAT proteins was decreased in CD27$^-$CD28$^-$CD8$^+$ T cells compared to expression of the same proteins in T_N CD8$^+$ cells (Fig. 1e), the mRNA levels for these TCR signaling components were similar in CD8$^+$ T_{EMRA} and CD8$^+$ T_N cells analyzed by scRNA-seq (not shown), which suggests that their expression might be regulated by post-translational modification in CD27$^-$CD28$^-$CD8$^+$ T cells. These observations suggest that CD8$^+$ T_{EMRA} cells have characteristics of cellular senescence and express a range of NKRs, NK adaptors and cytotoxic mediators.

NKG2D and DAP12 induce cytotoxicity in senescent CD8$^+$ T cells. We next investigated whether CD27$^-$CD28$^-$CD8$^+$ T cells had NK cell-like functions independently of TCR–MHC (major histocompatibility complex) interactions. On the basis of the expression of the degranulation marker CD107a[21], CD27$^-$CD28$^-$CD8$^+$ T cells killed K562 cells, an MHC class I–deficient tumor cell line, with the same efficiency as NK cells (Fig. 4a). These data were confirmed using a calcein-release assay (Extended Data Fig. 5a,b). To address whether NKG2D mediated the cytotoxic activity of CD27$^-$CD28$^-$CD8$^+$ T cells, we knocked down NKG2D in CD28$^-$CD8$^+$ T cells with a small interfering RNA (siRNA) specific for NKG2D (siNKG2D CD8$^+$T cells) and assessed their ability to kill MHC class I–deficient C1R cells transfected with the NKG2D ligand MICA*008 (C1R–MICA cells) when cocultured for 6 h (Extended Data Fig. 5c,d). CD28$^-$CD8$^+$T cells transfected with scrambled siRNA (siCtrl) as a control showed increased degranulation, measured by CD107a exposure, toward C1R–MICA compared to C1R cells, whereas the cytotoxicity of siNKG2D CD8$^+$ T cells toward the C1R–MICA cells was inhibited compared to siCtrl (Fig. 4b), which indicates that CD28$^-$CD8$^+$ T cells could kill target cells in a manner dependent on NKG2D.

Expression of NKG2D on the cell surface requires its association with adaptor proteins that stabilize the immunoreceptor complex and provide it with signaling activity[22]. NKG2D associates with the adaptor molecules DAP10 and DAP12. DAP10 contains a YxxM-motif that activates PI3K[23,24], while DAP12 has an ITAM-motif that can recruit and activate Zap70-Syk to trigger cytokine release and cytotoxicity[25–27]. In human CD8$^+$ T cells, NKG2D is predominantly associated with DAP10 (refs. [23,27]) (Extended Data Fig. 5e), which allows it to act as a costimulatory signal for the TCR. Immunoblot analysis (Fig. 4c) and intracellular flow cytometry (Fig. 4d) indicated increased expression of DAP12 in CD27$^-$CD28$^-$CD8$^+$ T cells compared to CD8$^+$ T_N cells, which corresponds to the transcriptomic data indicating that *Tyrobp* (which encodes DAP12) was strongly induced in CD8$^+$ T_{EMRA} cells compared to CD8$^+$ T_N cells. To investigate whether the killing activity of CD27$^-$CD28$^-$CD8$^+$ T cells was mediated by DAP12 association with NKG2D, we immunoprecipitated NKG2D from CD28$^+$C8$^+$ or CD28$^-$CD8$^+$ T cells isolated from the peripheral blood

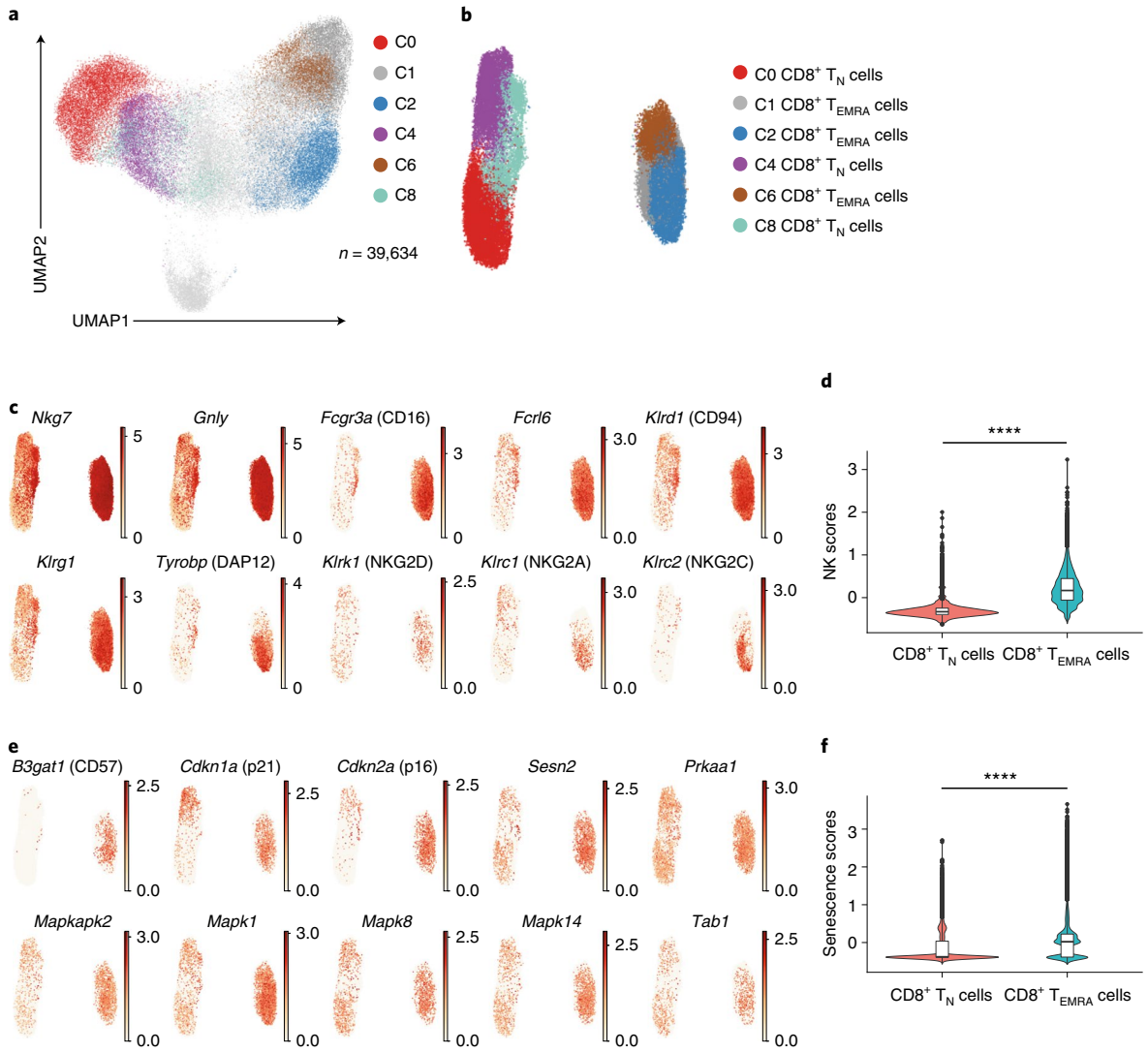

Fig. 3 | NK and senescence markers within T_N and T_{EMRA} cells. a, UMAP plot of single-cell sorted IL-7R$^+$CD8$^+$ and IL-7R$^-$CD8$^+$ T cells from six healthy older donors. Highlighted clusters were considered as T_N (C0, C4 and C8) and T_{EMRA} (C1, C2 and C6) compartments. **b**, UMAP plot showing reclustering of selected T_N (C0, C4, and C8) and T_{EMRA} (C1, C2, and C6) CD8$^+$ cells from **a** ($n = 39{,}634$ cells). **c**, UMAP plots representing the expression values of NK-related genes in reclustered T_N and T_{EMRA} CD8$^+$ cells from **b**. Scales show low expression (yellow) to high expression (red). **d**, Violin plots of NK-related gene expression determined by scRNA-seq in T_N and T_{EMRA} CD8$^+$ T cells clustered as in **b** (means, range and distribution of individual data; $n = 39{,}364$ single cells). **e**, UMAP plots showing expression of senescence-associated genes determined by scRNA-seq in T_N and T_{EMRA} CD8$^+$ T cells reclustered as in **b**. Scales show low expression (yellow) to high expression (red). Other aliases or CD numbers of some gene products are shown in brackets. **f**, Violin plots of senescence scores calculated on the basis of the average normalized expression of each senescence-associated gene across T_N and T_{EMRA} CD8$^+$ cells clustered as in **b** (means, range and distribution of individual data; $n = 39{,}364$ single cells). The gene lists used to define NK and senescence scores are given in Supplementary Table 4.

of healthy donors. DAP12 was found to associate with NKG2D only in the CD28$^-$CD8$^+$ T cells (Fig. 4e).

We next investigated whether ligation of NKG2D induced the phosphorylation of Zap70-Syk in CD27$^-$CD28$^-$CD8$^+$ T cells. CD3 ligation with a monoclonal antibody to CD3 induced the phosphorylation of Zap70-Syk, as expected, whereas using an NKG2D monoclonal antibody alone induced more p-Zap70 and p-Syk compared to using a CD3 monoclonal antibody alone (Fig. 4f), which indicates that CD27$^-$CD28$^-$CD8$^+$ T cells can be activated by both the TCR and NKG2D, but show an increased propensity to respond to the latter. NKG2D stimulation alone was sufficient to induce expression of granzyme B and secretion of the cytokine IFN-γ in CD27$^-$CD28$^-$CD8$^+$ T cells (Fig. 4g). siRNA-mediated silencing of DAP12 in CD28$^-$CD8$^+$ T cells impaired the cytolytic degranulation of CD28$^-$CD8$^+$ T cells toward C1R–MICA cells compared to scrambled siRNA control-transfected CD28$^-$CD8$^+$ T cells (Fig. 4h). Thus, DAP12 expression was upregulated in CD28$^-$CD8$^+$ T cells and was necessary and sufficient to mediate NKG2D-dependent cytotoxicity.

Sestrins block TCR signaling but increase NK receptors in CD8$^+$ T cells. CD27$^-$CD28$^-$CD8$^+$ T cells have reduced proliferative activity after TCR stimulation[4,5,7]. We investigated whether reduced expression of the components of the CD3–TCR complex compromised the efficiency of proximal TCR signaling. Phospho-flow cytometry indicated impaired phosphorylation of CD3ζ after stimulation with CD3 antibodies in CD27$^-$CD28$^-$CD8$^+$ T cells compared to CD27$^+$CD28$^+$CD8$^+$ T cells (Fig. 5a). Although the expression of total Zap70 was increased in CD28$^-$CD27$^-$CD8$^+$ T cells (Fig. 1e),

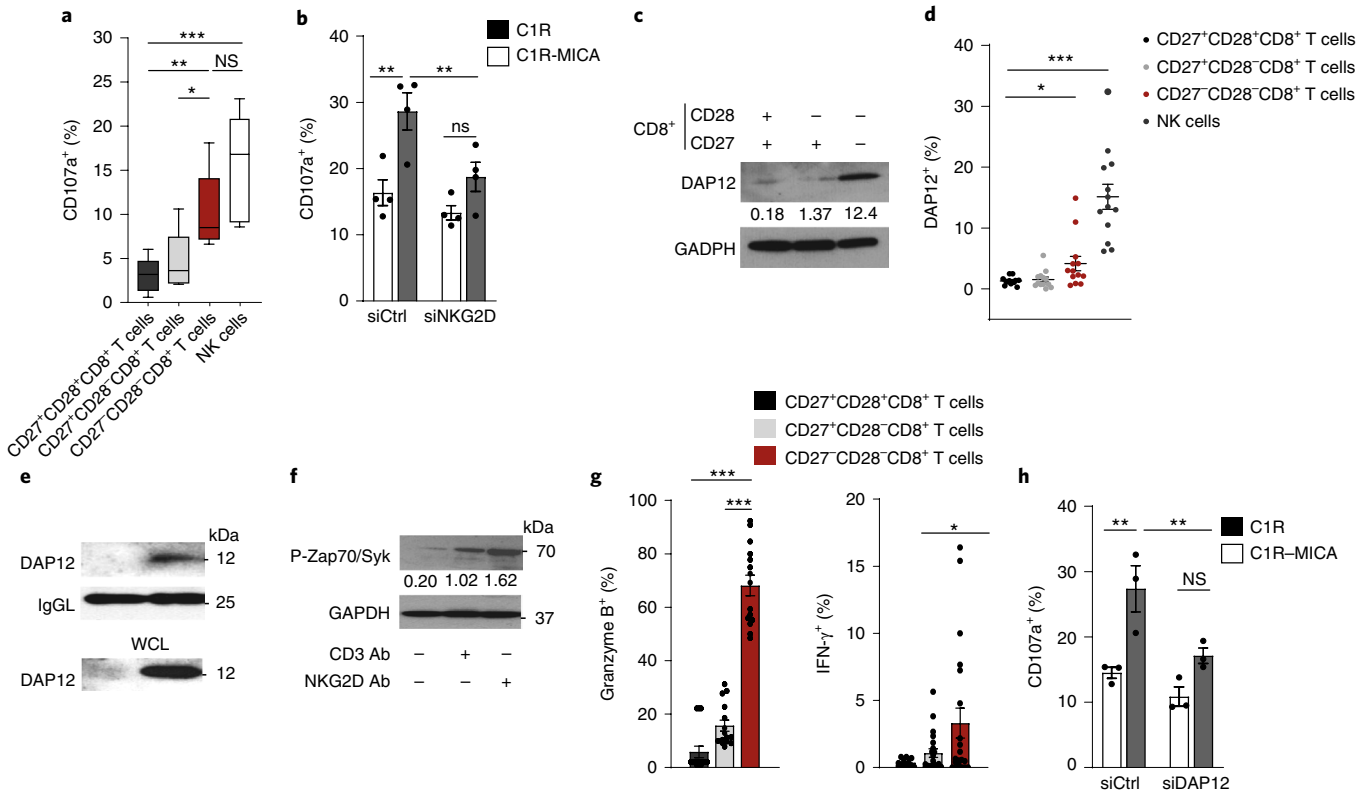

Fig. 4 | NKG2D–DAP12 complex mediates NK cytotoxicity in CD27⁻CD28⁻CD8⁺ T cells. a, Box-and-whisker plot of cell-surface CD107a expression of CD27⁺CD28⁺CD8⁺, CD27⁺CD28⁻CD8⁺, CD27⁻CD28⁻CD8⁺ and CD3⁻CD56⁺ NK cells isolated from healthy donors cocultured with K562 cells at an effector to target ratio (E:T) of 2:1 (median and range, $n=5$). NS, not significant. **b**, CD107a expression on CD28⁻CD8⁺ T cells transfected with NKG2D siRNA (siNKG2D) or siCtrl and cultured with C1R-MICA or C1R (E:T ratio 2:1) for 6 h (mean and s.e.m., $n=4$). **c**,**d**, Immunoblots (representative of five independent experiments with similar results) (**c**) and flow cytometry (**d**) (means and s.e.m., $n=12$) showing DAP12 expression on CD27⁺CD28⁺CD8⁺, CD27⁺CD28⁻CD8⁺, CD27⁻CD28⁻CD8⁺ and CD3⁻CD56⁺ NK cells. **e**, Expression of DAP12 in lysed CD28⁺CD8⁺ T cells and CD28⁻CD8⁺ T cells coimmunoprecipitated with antibody to NKG2D. Loading control, light chain IgG (IgGL). A whole-cell lysate (WCL) immunoblot is shown as a control. Results shown are representative of two independent experiments. **f**, Phosphorylation of Zap70(Tyr319) and Syk(Tyr352) in freshly isolated CD27⁻CD28⁻CD8⁺ T cells after treatment with CD3 monoclonal antibody (OKT3, 10 μg ml⁻¹, 15 min) and/or NKG2D Ab (1D11, 5 μg ml⁻¹, 15 min). Numbers indicate relative expression normalized to total expression of Zap70. Results shown are representative of two experiments. **g**, Granzyme B expression (left) and IFN-γ secretion (right) in CD27⁺CD28⁺CD8⁺, CD27⁺CD28⁻CD8⁺, and CD27⁻CD28⁻CD8⁺ T cells after stimulation with NKG2D antibody (5 μg ml⁻¹, means and s.e.m., $n=15$ donors). **h**, CD107a expression in human CD28⁻CD8⁺ T cells transfected with DAP12 siRNA (siDAP12) or siCtrl cultured with C1R-MICA or C1R cells for 6 h (E:T ratio 2:1; means and s.e.m., $n=4$). Statistical significance was determined with the Kruskal–Wallis test in **a**, the Friedman test with Dunn´s correction in **d**, a two-way ANOVA with Bonferroni correction in **b** and **j** and a one-way ANOVA with Tukey's multiple comparisons test in **g** (*$P<0.05$, **$P<0.01$, ***$P<0.001$).

its phosphorylation was impaired in these cells compared to that in CD28⁺CD27⁺CD8⁺ T cells following CD3 activation (Fig. 5b).

The stress-sensing sestrin proteins induce characteristics of senescence in CD4⁺ T cells by forming a complex with the kinase AMPK and the MAP kinases that inhibits signaling through the TCR[7]. Flow cytometry (Fig. 5c,d) and immunoblotting (Fig. 5e) indicated that human peripheral blood CD27⁻CD28⁻CD8⁺ T cells from young subjects (<40 y) exhibited increased expression of sestrin 1 and sestrin 2 compared to their expression in CD27⁺CD28⁺CD8⁺ T cells. Sestrin 2 was upregulated in total CD8⁺ T cells from donors older than 65 years compared to those between 18 and 35 years (Extended Data Fig. 5f). In addition, CD27⁻CD28⁻CD8⁺ T cells had increased amounts of activated Jnk MAP kinase (p-Jnk) compared to CD27⁺CD28⁺CD8⁺ T cells (Fig. 5e). Immunoprecipitation experiments indicated that DAP12, sestrin 2 and Jnk were associated with NKG2D in CD27⁻CD28⁻CD8⁺ T cells (Fig. 6a), whereas imaging cytometry indicated that sestrin 2, DAP12 and p-Jnk colocalized in CD27⁻CD28⁻CD8⁺ T cells, but not in CD8⁺ T_N cells (Fig. 6b,c). These observations suggest that sestrin 2 associates with NKG2D-DAP12-Jnk in CD27⁻CD28⁻CD8⁺ cells.

Next, we tested whether sestrins regulated the expression of NKG2D in human CD28⁻CD8⁺ T cells. Peripheral blood CD28⁻CD8⁺ T cells isolated from healthy donors (median age, 39 y; range, 25–70 y) were lentivirally transduced with short hairpin RNA (shRNA) against sestrin 1, sestrin 2 and sestrin 3 (shSesn) had significantly reduced expression of DAP12 (Fig. 6d) and NKG2D compared to CD28⁻CD8⁺ T cells transduced with control vectors (Fig. 6e), which indicates that sestrins modulate the expression of NKG2D in these cells. siRNA-mediated depletion of Jnk (Fig. 6f) or its inhibition with the small molecule inhibitor SP-600125 in CD28⁻CD8⁺ T cells (Fig. 6g) reduced the expression of NKG2D, increased the frequency of CD28⁺ cells and restored proximal TCR signaling following CD3 ligation compared to untreated CD28⁻CD8⁺ T cells (Fig. 6f,g). This indicated a reconstitution of T cell-related functions, which implies that sestrins may act through Jnk to induce expression of NKG2D expression in CD28⁻CD8⁺ T cells.

Yellow fever virus induces the upregulation of NK receptors on CD8⁺ T cells. We then tested whether the upregulation of NKRs by CD8⁺ T cells occurred exclusively as a result of cellular senescence

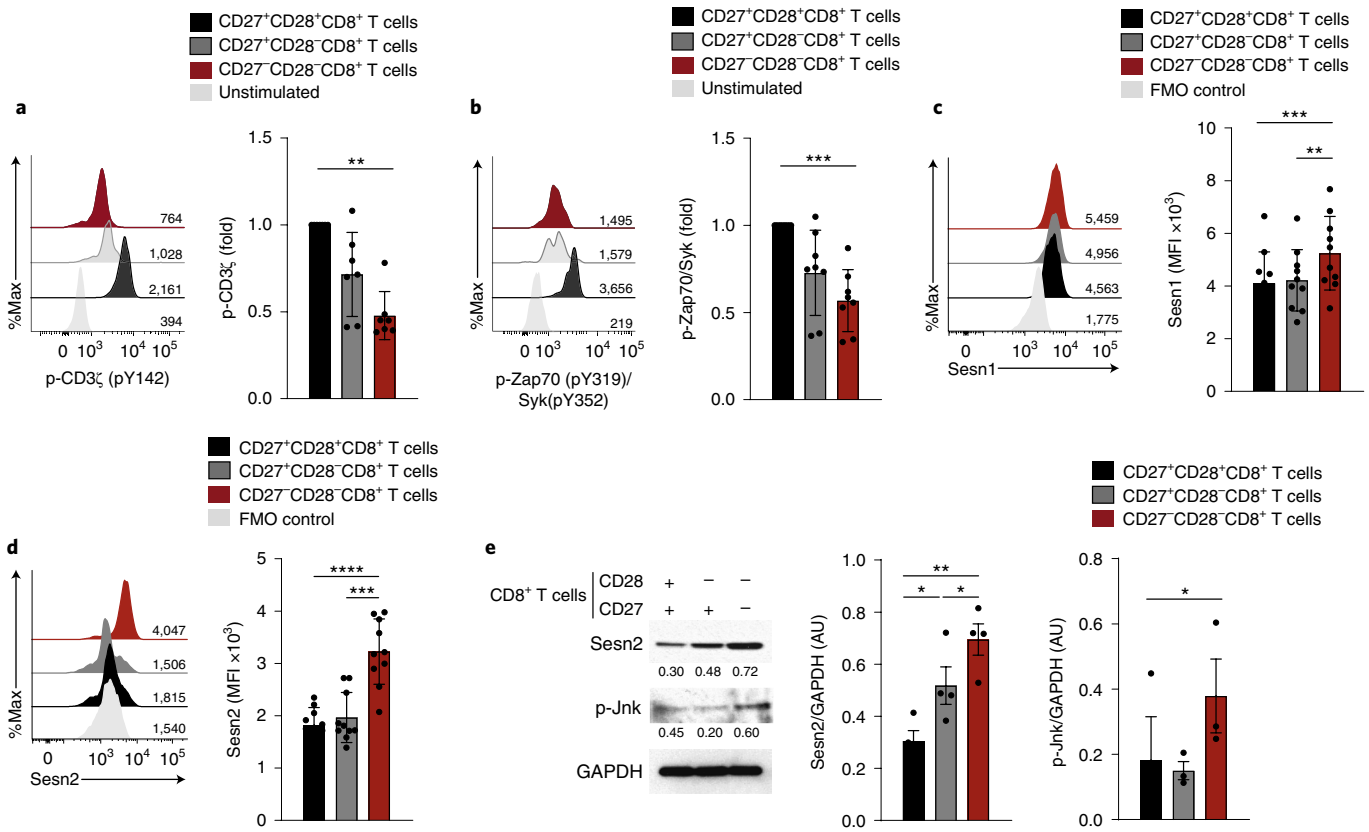

Fig. 5 | Sestrins and Jnk MAPK dampen TCR signaling in CD27⁻CD28⁻CD8⁺ T cells. a, Representative histograms of p-CD3ζ in CD27⁺CD28⁺CD8⁺, CD27⁺CD28⁻CD8⁺, and CD27⁻CD28⁻CD8⁺ T cells stimulated with anti-CD3 antibody (OKT3, 10 μg ml⁻¹, 15 min). Unstimulated CD27⁺CD28⁺CD8⁺ T cells are shown as a control. Numbers on histograms represent the mean fluorescence intensity (MFI) for each subset. Summary data are given (means and s.d., $n = 8$ donors). **b**, Representative histograms of p-Zap70 and p-Syk in CD27⁺CD28⁺CD8⁺, CD27⁺CD28⁻CD8⁺ and CD27⁻CD28⁻CD8⁺ T cells stimulated as in **a**. Unstimulated CD27⁺CD28⁺CD8⁺ T cells are shown as a control. Numbers on histograms represent the MFI for each subset. Summary data are given (means and s.d., $n = 8$). Summary results are presented as the MFI relative to that of CD27⁺CD28⁺CD8⁺ T cells, set to 1. **c**,**d**, Expression of Sesn1 (**c**) and Sesn2 (**d**) proteins determined by flow cytometry in CD27⁺CD28⁺CD8⁺, CD27⁺CD28⁻CD8⁺ and CD27⁻CD28⁻CD8⁺ T cells (means and s.d., $n = 10$ donors). **e**, Immunoblot of Sesn2 and p-Jnk (T183/Y185) expression in CD27⁺CD28⁺CD8⁺, CD27⁺CD28⁻CD8⁺ and CD27⁻CD28⁻CD8⁺ T cells, freshly isolated from the peripheral blood of healthy donors. Immunoblot is representative of three independent experiments with similar results. Densitometry data from immunoblots for all donors is also shown (means and s.e.m., $n = 3$ donors for p-Jnk, $n = 4$ donors for Sesn2). Statistical significance was determined by ANOVA with the Friedman test and Dunn's post-test correction in **a** and **b** and by a repeated measures one-way ANOVA with Tukey's multiple comparisons test in **c**–**e** (*$P < 0.05$, **$P < 0.01$, ***$P < 0.001$, ****$P < 0.0001$. FMO, fluorescence minus one control.

or whether NKRs were expressed on less-differentiated subsets of CD8⁺ T cells in response to antigenic stimulation, and whether the expression was maintained as cells differentiated toward senescence. Using publicly available RNA-seq gene expression data that was generated in a cohort of 12 individuals who had received the yellow fever virus (YFV) vaccine[28], we compared CD8⁺ T effector (T_E cells), defined as CD8⁺ YFV-tet⁺ cells that were present at day 14 post vaccine, and CD8⁺ T memory (T_M cells) defined as CD8⁺ YFV-tet⁺ cells that were present 4–13 years post vaccine, to YFV-tet⁻CD8⁺ T_N cells. Cytotoxic mediator genes, such as *Fasl*, *Prf1*, *Gzma* and *Gzmb*, were highly expressed in CD8⁺ T_E cells and CD8⁺ T_M cells compared to CD8⁺ T_N cells (Extended Data Fig. 6). Additionally, there was a significant upregulation of multiple NKR-encoding genes, including *Kir*, *Fcgr3a*, *Cd57* and *Klrc1* in CD8⁺ T_E cells and CD8⁺ T_M cells compared to those in CD8⁺ T_N cells, as well as chemokine receptor genes (*S1pr5*, *Cmklr1* and *Cx3cr1*) and genes that encoded NK adaptor proteins, such as *Tyrobp* (Extended Data Fig. 6). The upregulation of these genes occurred in YFV-tet⁺CD8⁺ T_E cells during the effector phase of the response and was maintained in long-lived YFV-tet⁺ T_M cells (Extended Data Fig. 6). According to published data, YFV-tet⁺ T_M cells lack markers of senescence, such as CD57, are CD27⁺CD28⁺ and are polyfunctional with regard to cytokine secretion[29]. Unlike the CD8⁺ T_{EMRA} cells, YFV-tet⁺CD8⁺ T_M cells exhibit proliferative potential in vitro, which suggests that they are not terminally differentiated[29]. YFV-tet⁺CD8⁺ T_E and T_M cells showed slight downregulation of the TCR signalosome (enocded by genes such as *Lat, Plcg1, Zap70*) compared to CD8⁺ T_N cells (Extended Data Fig. 6). Of note, expression of the gene encoding sestrin 2 was upregulated in the YFV-tet⁺CD8⁺ T_E and T_M cells compared to CD8⁺ T_N cells (Extended Data Fig. 6). This analysis indicated that the expression of NKRs on CD8⁺ T cells was not limited to senescent CD27⁻CD28⁻CD8 T cells but was also a feature of YFV-tet⁺CD8⁺ T_E and T_M cells after activation in vivo.

Sestrins regulate the function of CD8⁺ T cells in vivo. Sestrins are known to regulate the decrease in function of CD4⁺ T cells in aged mice and humans[7]. We next investigated whether sestrins directly regulated the expression of NKRs in CD8⁺ T cells in young (~6 weeks) and old (~18 months) wild-type (WT) mice and old (~18 months) *Sesn1*$^{-/-}$ and *Sesn2*$^{-/-}$ mice. Mice were vaccinated subcutaneously against methylated BSA (mBSA) and were rechallenged with mBSA in the footpad two weeks later to induce a delayed-type

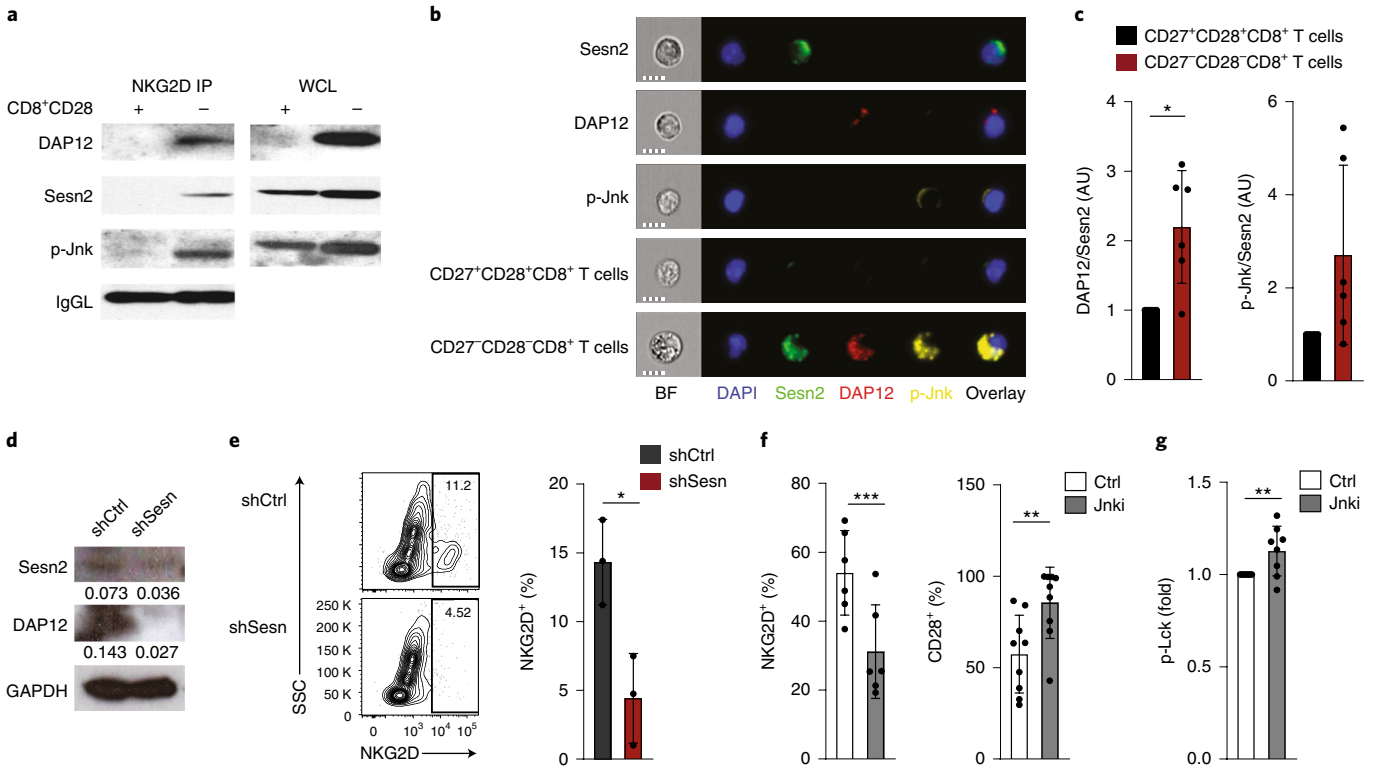

Fig. 6 | Sestrins regulate DAP12 and NKG2D expression in CD8⁺ T cells. a, Expression of DAP12, sestrin 2 and p-Jnk (T183/Y185) in lysed CD28⁺CD8⁺ T cells and CD28⁻CD8⁺ T cells immunoprecipitated with NKG2D. Loading control is IgG light chain (IgGL). Results are representative of two independent experiments. **b**, Cellular localization of Sesn2 (AF488, green), DAP12 (PE, red) and p-Jnk (T183/Y185, AF647, yellow) in CD27⁺CD28⁺CD8⁺ and CD27⁻CD28⁻CD8⁺ T cells. 'Sesn2', 'DAP12', and 'p-Jnk' denote single stain controls in CD27⁻CD28⁻CD8⁺. Nuclei are stained with DAPI (blue). BF, brightfield; scale bars, 7 µm. **c**, Overlap of Sesn2 and DAP12 or p-Jnk in CD27⁺CD28⁺CD8⁺ and CD27⁻CD28⁻CD8⁺ T cells. Bright detail similarity scores that exceeded 2 were considered to be overlapping. Data are normalized to the CD27⁺CD28⁺CD8⁺ T cell subset for each donor (means and s.d., $n = 6$). AU, arbitrary units. **d**,**e**, Isolated human CD8⁺CD28⁻ T cells were transduced with control (shCtrl) or anti-sestrin (shSesn) vectors. **d**, Immunoblot for Sesn2 and DAP12, representative of two experiments. **e**, Representative contour plots and summary data of NKG2D expression. Results are presented relative to cells that were transduced with shCtrl for each donor, set as 1 (means and s.d., $n = 3$ donors). **f**, Frequency of NKG2D and CD28 in isolated CD28⁻CD8⁺ T cells treated with siJnk (means and s.d., $n = 6$ donors). **g**, Lck phosphorylation in CD28⁻CD8⁺ T cells that were pretreated with Jnk inhibitor (SP-600125, 10 µM) prior to anti-CD3 stimulation (OKT3, 10 µg ml^{-1}, 15 min; means and s.d., $n = 8$ donors). Statistical significance was determined by two-tailed paired Student's *t*-tests in **c**,**f**–**g**) (*$P < 0.05$, **$P < 0.01$, ***$P < 0.001$).

hypersensitivity (DTH) response as an index of successful immune induction. All mice mounted a DTH response to the rechallenge, but the DTH response in old WT, *Sesn1*$^{-/-}$ and *Sesn2*$^{-/-}$ mice resulted in increased footpad swelling compared to that in young WT mice (Fig. 7a). The response resolved more slowly in old WT compared to young WT mice, whereas the response in old *Sesn1*$^{-/-}$ and *Sesn2*$^{-/-}$ mice resolved faster than that in old WT mice (Fig. 7a,b). Spleen weights were equivalent in all groups post mBSA challenge (Extended Data Fig. 7a). There were no changes in the proportions of splenic NK cells, invariant NKT (iNKT) cells, CD4⁺ T cells and CD8⁺ T cells in all old and young mice following the DTH response (Extended Data Fig. 7b,c). However, CD44⁺CD62L⁻CD8⁺ T effector cells (T_{EFF} cells) increased in number, whereas the number of CD44⁻CD62L⁺CD8⁺ T_N cells decreased in old WT mice, but not in old *Sesn1*$^{-/-}$ and *Sesn2*$^{-/-}$ mice, compared to young WT mice (Extended Data Fig. 7d,e).

Expression of NKG2D and DAP12, as well as NKG2A, NKG2C, NKG2E and Ly49, was higher on the CD8⁺ T cells from the old WT mice compared to young WT mice, whereas expression of these proteins was lower in old *Sesn1*$^{-/-}$ and *Sesn2*$^{-/-}$ mice compared to old WT mice (Fig. 7c–e and Extended Data Fig. 7f), which suggests that the expression of these receptors is modulated by sestrins. Importantly, the expression of NKG2D, as well as NKG2A, NKG2C and NKG2E on CD3⁻TCRβ⁻NK1.1⁺ NK cells or TCRβ⁺CD1d-tet⁺ iNKT cells was similar in young WT, old WT and old *Sesn1*$^{-/-}$ and *Sesn2*$^{-/-}$ mice (Fig. 7f), which indicates that sestrins uniquely regulate the expression of NKRs in CD8⁺ T cells. To examine the effect of sestrin deficiency on the cytotoxic function of CD8⁺ T cells in vivo, 24-month-old WT mice and 24-month-old *Sesn1*$^{-/-}$; *Sesn2*$^{-/-}$; *Sesn3*$^{+/-}$ mice were depleted of NK cells by intraperitoneal treatment with anti-NK1.1 prior to intravenous injection of equal numbers of 5TGM1 myeloma cells expressing Rae-1, the mouse equivalent of MICA/B, and Rae-1⁻ splenocytes. Six hours post transfer of target cells, more Rae-1⁺ 5TGM1 cells were detected in the spleens of *Sesn1*$^{-/-}$; *Sesn2*$^{-/-}$; *Sesn3*$^{+/-}$ mice compared to those of WT mice (Fig. 7g). This resulted from decreased specific lysis of Rae-1⁺ 5TGM1 target cells in *Sesn1*$^{-/-}$; *Sesn2*$^{-/-}$; *Sesn3*$^{+/-}$ mice compared to WT mice (Fig. 7g). These observations indicate that the sestrins regulate the expression of NKG2D and DAP12 and confer NK cell-like cytotoxic activity to CD8⁺ T cells of old mice in vivo.

Discussion

Here we provide phenotypic, functional and mechanistic data to indicate that as CD8⁺ T cells differentiated toward senescence they lost the expression of costimulatory molecules such as CD28 and CD27 and downregulated TCR signaling molecules such as Lck

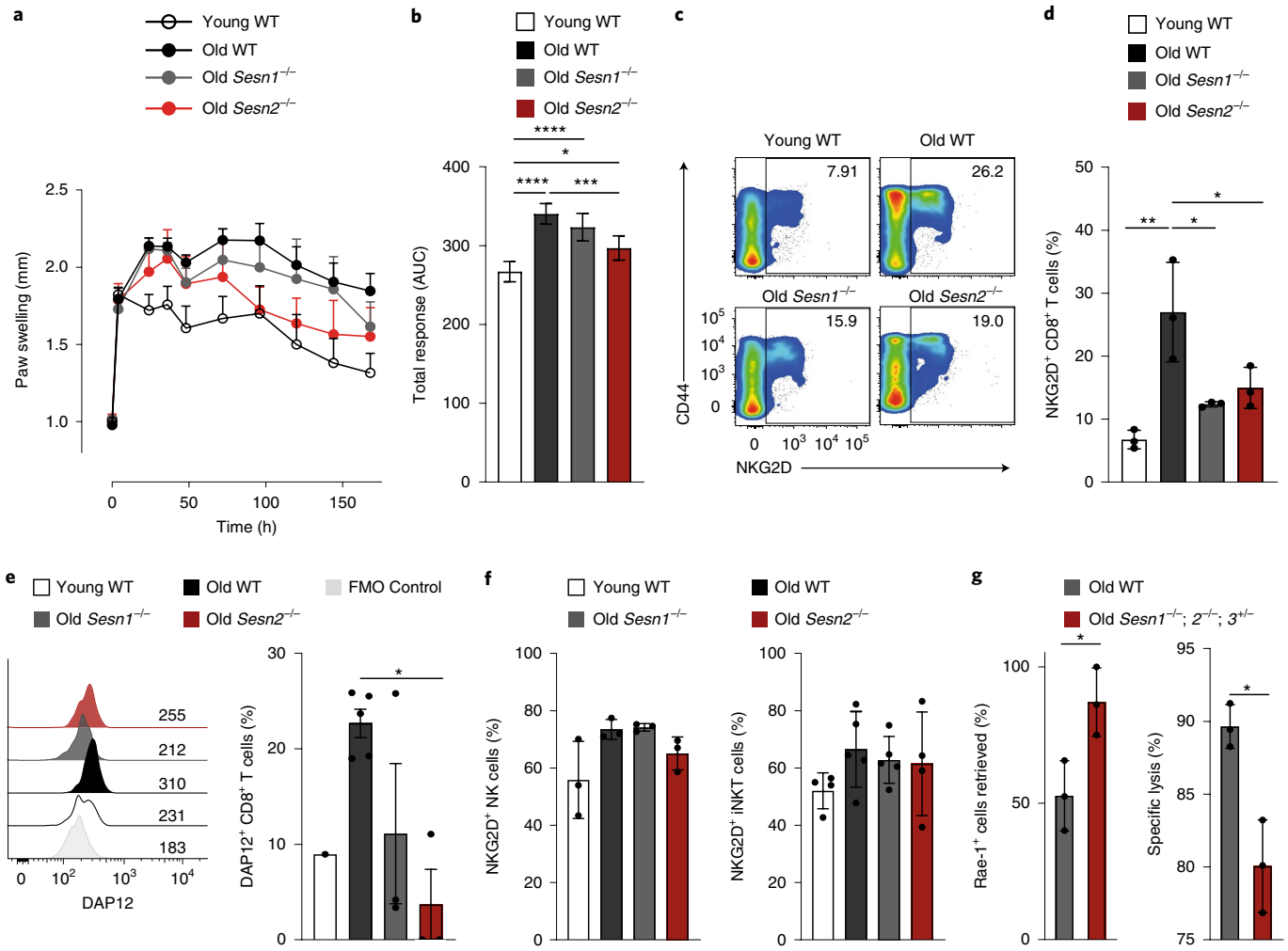

Fig. 7 | Sestrins induce an age-dependent NK phenotype in CD8⁺ T cells in vivo. a, Measurement of paw size (normalized to the contralateral, PBS control paw) over time (0 h, 4 h, 24 h, 36 h, 2 d, 3 d, 4 d, 5 d, 6 d and 7 d) in young WT ($n=4$), old WT ($n=10$), old *Sesn1*$^{-/-}$ ($n=5$) and old *Sesn2*$^{-/-}$ ($n=4$) mice following intraplantar treatment with methylated BSA (mBSA). **b**, Area under the curve (AUC) integration of the time course data shown in **a** (means and s.d.) **c**, Representative pseudocolor density plots showing CD44 versus NKG2D expression on TCRβ⁺CD3⁺CD8⁺ T cells isolated from spleens of young WT, old WT, old *Sesn1*$^{-/-}$ and old *Sesn2*$^{-/-}$ mice. Frequencies of parent gates are shown in the top right-hand corner. **d**, Cumulative data of NKG2D expression in splenic TCRβ⁺CD3⁺CD8⁺ T cells from young WT, old WT, old *Sesn1*$^{-/-}$ and old *Sesn2*$^{-/-}$ mice ($n=3$ mice per group). **e**, Representative histogram of DAP12 expression from splenic TCRβ⁺CD3⁺CD8⁺ T cells from young WT, old WT, old *Sesn1*$^{-/-}$, and old *Sesn2*$^{-/-}$ mice. FMO control is shown. Cumulative data shown ($n=3$ per group, $n=1$ young WT). **f**, NKG2D expression in splenic NK and iNKT cells from the same mice as in **c**–**d** (means and s.d., $n=3$ mice per group). **g**, Retrieval of Rae-1⁺ 5TGM1 cells as a fraction of injected cells (left panel) and killing and specific lysis of injected Rae-1⁺ 5TGM1 cells (right panel) from the spleens of NK-depleted (24 h after anti-NK1.1 intraperitoneal injection) old WT and old *Sesn1*$^{-/-}$; *Sesn2*$^{-/-}$; *Sesn3*$^{+/-}$ mice 6 h after intravenous challenge (means and s.d., $n=3$ mice per group). Statistical significance was determined with one-way ANOVA with Tukey's multiple comparisons test in **b**,**d**–**f** and with two-tailed unpaired Student's *t*-tests in **g**. (*$P<0.05$, **$P<0.01$, ***$P<0.001$, ****$P<0.0001$).

and LAT, while the expression of NKRs such as NKG2D, NKG2A and CD16 wsa upregulated. Compared to CD28⁺CD27⁺CD8⁺ T cells, CD28⁻CD27⁻CD8⁺ T cells acquired a senescent phenotype. Expression of NKRs was associated with acquisition of the ability to kill tumor cells in vitro and in vivo through an NKR-dependent process. The downregulation of TCR-related signaling molecules concomitant with the acquisition of NKR-related molecules was regulated by sestrins.

Altered TCR signaling pathways in iNKT and antigen-specific CD8⁺ T cells result in the development of unconventional functions that are not restricted to TCR–MHC interactions[30,31]. The suppression of TCR signaling, along with an acquired responsiveness to innate stimuli was proposed to be a characteristic that defines innate-like T cells[32]. Here, we found that the TCR to NKR functional switch in CD8⁺ T cells was dependent on the kinase Jnk, similar to previous findings in CD4⁺ T cells[7]. The mechanism by which sestrins modulate this transition remains unclear. Experiments in sestrin-deficient mice indicated that sestrins did not regulate the expression of NKRs in NK cells or iNKT cells, and it remains unclear whether sestrins may regulate the function of other types of innate-like T cells, such as γδ T cells.

The reprogramming of CD27⁻CD28⁻CD8⁺ T cells from TCR to NKR functional activity could be particularly relevant for CD8⁺ T cells specific for persistent pathogens, such as cytomegalovirus and Epstein-Barr virus, which accumulate during aging[33–35]. Our data suggest that in addition to their role in maintaining long-term specific immunity against these viruses, these cells may also recognize virus-infected cells or tumor cells in an NK cell-like, antigen-independent manner, thus enabling them to exhibit broad protective functions.

Our observations raise questions about the biological significance of such changes and the possible advantage of generating T cells with NK cell-like characteristics. The accumulation of $CD8^+$ T_{EMRA} cells was reported to be a predictor of successful aging[8]. One reason for this may be that acquisition of NKRs by $CD8^+$ T_{EMRA} cells might allow them to broaden their capacity for immune surveillance by utilizing different recognition systems, thereby partly compensating for decreased output of T_N cells in older subjects and reduced TCR-mediated classical T cell function[36]. Given the increased burden of tumors and infections with age, the expansion of NK cell-like functions in $CD8^+$ T cells could be an advantageous adaptation that would enable the recognition of transformed cells.

Senescent cells are pro-inflammatory and increase in number in many tissues during aging[37,38]. The removal of these senescent cells from aged tissue enhances organ function and retards age-related functional decline[39,40]. Because NK cells and $CD8^+$ T cells can recognize and kill senescent cells via NKG2D-mediated mechanisms[9,10,41], NKR-expressing $CD27^-CD28^-CD8^+$ T cells may participate in the surveillance and elimination of senescent cells in aged tissue. Given the observations here that sestrins regulate functional fate decisions in T cells, it will be important to identify whether these molecules also have similar roles in other cell types.

It is important to know when the expression of sestrins and NKRs is induced on T cells after vaccination. Gene expression studies in YFV-specific $CD8^+$ T cells from previously non-immunized young individuals (<40 y) vaccinated with YFV showed that expression of NKRs and sestrins was upregulated in the effector phase of the response (2 weeks post vaccination) and was maintained in the $CD8^+$ T_M cells for years afterwards[28,29]. This indicates that sestrins are not only induced when $CD27^-CD28^-CD8^+$ T cells become senescent. Naive $CD27^+CD28^+$ T cells within the CD4 compartment of older individuals (>65 y) have been shown to express a significantly higher level of sestrins than have naive $CD27^+CD28^+CD4^+$ T cells from young individuals[7] suggesting that this molecule will have an impact on vaccine responses, which induce the expansion of naive T cell precursors, during aging. It is not clear whether naive YFV-specific $CD8^+$ T cell precursors in older humans express higher levels of sestrins and whether these cells can be activated optimally after vaccination. Nevertheless, it has been shown that in old mice, sestrin inhibition can enhance the number of influenza-specific $CD4^+$ T cells after influenza vaccination in vivo[7]. This may be a strategy to also enhance the response to other vaccines during aging. A caveat is that the long-term blockade of sestrins either with specific inhibitors or by transfection with inhibitory shRNA may be dangerous, as it could enhance the proliferation of senescent-like T cells that harbor DNA damage. However, the temporary blockade of sestrins may be a safe strategy to increase the number of antigen-specific T cells after vaccination to enhance immunity during aging[7].

Online content

Any methods, additional references, Nature Research reporting summaries, source data, extended data, supplementary information, acknowledgements, peer review information; details of author contributions and competing interests; and statements of data and code availability are available at https://doi.org/10.1038/s41590-020-0643-3.

Received: 30 July 2019; Accepted: 26 February 2020;
Published online: 30 March 2020

References

1. Akbar, A. N., Beverley, P. C. & Salmon, M. Will telomere erosion lead to a loss of T-cell memory? *Nat. Rev. Immunol.* **4**, 737–743 (2004).
2. Gray, D. A role for antigen in the maintenance of immunological memory. *Nat. Rev. Immunol.* **2**, 60–65 (2002).
3. Mitri, D. et al. Reversible senescence in human $CD4^+CD45RA^+CD27^-$ memory T cells. *J. Immunol.* **187**, 2093–2100 (2011).
4. Henson, S. M. et al. p38 signaling inhibits mTORC1-independent autophagy in senescent human $CD8^+$ T cells. *J. Clin. Invest.* **124**, 4004–4016 (2014).
5. Lanna, A., Henson, S. M., Escors, D. & Akbar, A. N. The kinase p38 activated by the metabolic regulator AMPK and scaffold TAB1 drives the senescence of human T cells. *Nat. Immunol.* **15**, 965–972 (2014).
6. Tarazona, R. et al. Increased expression of NK cell markers on T lymphocytes in aging and chronic activation of the immune system reflects the accumulation of effector/senescent T cells. *Mech. Ageing Dev.* **121**, 77–88 (2001).
7. Lanna, A. et al. A sestrin-dependent Erk-Jnk-p38 MAPK activation complex inhibits immunity during aging. *Nat. Immunol.* **18**, 354–363 (2017).
8. Dunne, P. J. et al. Quiescence and functional reprogramming of Epstein–Barr virus (EBV)-specific $CD8^+$ T cells during persistent infection. *Blood* **106**, 558–565 (2005).
9. Pereira, B. I. et al. Senescent cells evade immune clearance via HLA-E-mediated NK and $CD8^+$ T cell inhibition. *Nat. Commun.* **10**, 2387 (2019).
10. Krizhanovsky, V. et al. Senescence of activated stellate cells limits liver fibrosis. *Cell* **134**, 657–667 (2008).
11. Dominguez, C. X. et al. The transcription factors ZEB2 and T-bet cooperate to program cytotoxic T cell terminal differentiation in response to LCMV viral infection. *J. Exp. Medicine* **212**, 2041–2056 (2015).
12. Kovalovsky, D. et al. PLZF induces the spontaneous acquisition of memory/effector functions in T cells independently of NKT cell-related signals. *J. Immunol.* **184**, 6746–6755 (2010).
13. Raberger, J. et al. The transcriptional regulator PLZF induces the development of CD44 high memory phenotype T cells. *Proc. Natl Acad. Sci. USA* **105**, 17919–17924 (2008).
14. Liu, D. et al. Integrin-dependent organization and bidirectional vesicular traffic at cytotoxic immune synapses. *Immunity* **31**, 99–109 (2009).
15. Bernardini, G., Sciumè, G. & Santoni, A. Differential chemotactic receptor requirements for NK cell subset trafficking into bone marrow. *Front. Immunol.* **4**, 12 (2013).
16. van Lier, R. A., ten Berge, I. J. & Gamadia, L. E. Human $CD8^+$ T-cell differentiation in response to viruses. *Nat. Rev. Immunol.* **3**, 931–939 (2003).
17. Rufer, N. et al. Ex vivo characterization of human $CD8^+$ T subsets with distinct replicative history and partial effector functions. *Blood* **102**, 1779–1787 (2003).
18. Henson, S. M. et al. KLRG1 signaling induces defective Akt (ser^{473}) phosphorylation and proliferative dysfunction of highly differentiated $CD8^+$ T cells. *Blood* **113**, 6619–6628 (2009).
19. Plunkett, F. J. et al. The loss of telomerase activity in highly differentiated $CD8^+CD28^-CD27^-$ T cells is associated with decreased Akt (Ser^{473}) phosphorylation. *J. Immunol.* **178**, 7710–7719 (2007).
20. Henson, S. M., Riddell, N. E. & Akbar, A. N. Properties of end-stage human T cells defined by CD45RA re-expression. *Curr. Opin. Immunol.* **24**, 476–481 (2012).
21. Aktas, E., Kucuksezer, U., Bilgic, S., Erten, G. & Deniz, G. Relationship between CD107a expression and cytotoxic activity. *Cell. Immunol.* **254**, 149–154 (2009).
22. Lanier, L. L. NKG2D receptor and its ligands in host defense. *Cancer Immunol. Res.* **3**, 575–582 (2015).
23. Wu, J. et al. An activating immunoreceptor complex formed by NKG2D and DAP10. *Science* **285**, 730–732 (1999).
24. Upshaw, J. L. et al. NKG2D-mediated signaling requires a DAP10-bound Grb2-Vav1 intermediate and phosphatidylinositol-3-kinase in human natural killer cells. *Nat. Immunol.* **7**, 524–532 (2006).
25. Diefenbach, A. et al. Selective associations with signaling proteins determine stimulatory versus costimulatory activity of NKG2D. *Nat. Immunol.* **3**, 1142–1149 (2002).
26. Gilfillan, S., Ho, E. L., Cella, M., Yokoyama, W. M. & Colonna, M. NKG2D recruits two distinct adapters to trigger NK cell activation and costimulation. *Nat. Immunol.* **3**, 1150–1155 (2002).
27. Wu, J., Cherwinski, H., Spies, T., Phillips, J. H. & Lanier, L. L. Dap10 and Dap12 form distinct, but functionally cooperative, receptor complexes in natural killer cells. *J. Exp. Med.* **192**, 1059–1068 (2000).
28. Akondy, R. S. et al. Origin and differentiation of human memory CD8 T cells after vaccination. *Nature* **552**, 362–367 (2017).
29. Akondy, R. S. et al. The yellow fever virus vaccine induces a broad and polyfunctional human memory $CD8^+$ T cell response. *J. Immunol.* **183**, 7919–7930 (2009).
30. Wang, X. et al. Human invariant natural killer T cells acquire transient innate responsiveness via histone H4 acetylation induced by weak TCR stimulation. *J. Exp. Med.* **209**, 987–1000 (2012).
31. Mingueneau, M. et al. Loss of the LAT adaptor converts antigen-responsive T cells into pathogenic effectors that function independently of the T cell receptor. *Immunity* **31**, 197–208 (2009).
32. Wencker, M. et al. Innate-like T cells straddle innate and adaptive immunity by altering antigen-receptor responsiveness. *Nat. Immunol.* **15**, 80–87 (2014).

33. Pawelec, G. Immunosenenescence: role of cytomegalovirus. *Exp. Gerontol.* **54**, 1–5 (2014).
34. Khan, N. et al. Herpesvirus-specific CD8 T cell immunity in old age: cytomegalovirus impairs the response to a coresident EBV infection. *J. Immunol.* **173**, 7481–7489 (2004).
35. Jackson, S. E. et al. CMV immune evasion and manipulation of the immune system with aging. *Geroscience* **39**, 273–291 (2017).
36. Vallejo, A. N. et al. Expansions of NK-like αβT cells with chronologic aging: novel lymphocyte effectors that compensate for functional deficits of conventional NK cells and T cells. *Ageing Res. Rev.* **10**, 354–361 (2011).
37. Coppé, J.-P. et al. Senescence-associated secretory phenotypes reveal cell-nonautonomous functions of oncogenic RAS and the p53 tumor suppressor. *PLoS Biol.* **6**, 2853–2868 (2008).
38. Campisi, J. & di Fagagna, F. Cellular senescence: when bad things happen to good cells. *Nat. Rev. Mol. Cell Biol.* **8**, 729–740 (2007).
39. Baker, D. J. et al. Naturally occurring $p16^{Ink4a}$-positive cells shorten healthy lifespan. *Nature* **530**, 184–189 (2016).
40. Baker, D. J. et al. Clearance of $p16^{Ink4a}$-positive senescent cells delays ageing-associated disorders. *Nature* **479**, 232–236 (2011).
41. Sagiv, A. et al. NKG2D ligands mediate immunosurveillance of senescent cells. *Aging* **8**, 328–344 (2016).

Methods

Study design. The study protocol was approved by the Ethical Committee of the Royal Free and University College London Medical School (Research Ethics number: 11/0473). Written informed consent was obtained from all study participants. Donors did not have any comorbidity, were not on any immunosuppressive drugs, and retained physical mobility and lifestyle independence. For analyses involving the $CD8^+$ T cell, IL-$7R^+$/IL-$7R^-$ single-cell data set studies were conducted following approval by the Institutional Review Board (IRB) of the University of Connecticut Health Center (IRB 14-194J-3). After receiving informed consent, blood samples were obtained from 6 healthy research volunteers (>65 years old) residing in the Greater Hartford, CT, region using services of the University of Connecticut Center on Aging Recruitment and Community Outreach Research Core and following previously published screening criteria[42].

Cell isolation and transfection. PBMCs were isolated by density gradient (Ficoll–Hypaque, Amersham Biosciences) from heparinized blood of healthy donors ($n = 22$, 26–83 y). Untouched NK and $CD8^+$ T cells were freshly isolated by magnetic activated cell sorting (MACS, Miltenyi Biotec) using a negative selection procedure. For microarray analysis, high-purity $CD8^+$ T cell subsets were sorted on the basis of CD27 and CD45RA expression[43], using a FACSAria flow cytometer (BD Biosciences). For functional assays, $CD8^+$ T cell subsets were freshly isolated according to CD27/CD28 expression by MACS, which identified analogous subsets but provided higher yields of viable cells (>95% purity) as described previously[5,7]. Double negative cells were obtained by complete negative isolation. We found that <1% of cells within these isolated populations expressed iNKT markers. Mucosal-associated invariant T cells (MAIT) cells express TCR Vα7.2 and these cells constitute ~5% of the peripheral $CD8^+$ T cell pool in humans[44]. We found 4% (range, 1–7.5%) of these cells in the isolated $CD28^+CD27^+CD8^+$ T cell population, 3% (range, 1–6.4) in the isolated $CD28^-CD28^+CD8^+$ T cell population and 2.9% (range, 1–4.9%) in the isolated $CD28^-CD27^-CD8^+$ T cell population. The results obtained are therefore unlikely to be due to contaminating iNKT or MAIT cells in our $CD8^+$ T cell populations.

Where indicated, freshly purified human $CD8^+$ T cells were transfected with siRNA for NKG2D (Santa Cruz Biotechnology, sc-42948) or DAP12 (sc-35172) by electroporation using the Amaxa Human NK Cell Nucleofector Kit and Nucleofector technology (Lonza), according to the manufacturer's instructions. A scrambled control siRNA (sc-37007) was used throughout. Efficiency of siRNA transfection was confirmed by measuring the expression of the protein of interest using flow cytometry, 36–48 h after transfection.

Microarray data acquisition. Cells purified by FACS were stimulated for 2 h with 0.5 μg ml^{-1} plate-coated anti-CD3 antibody (OKT3) and 5 ng ml^{-1} rhIL-2 before RNA isolation using the ARCTURUS PicoPure Isolation Kit (Thermo Fisher Scientific). The concentration of small quantities of RNA was determined using Nanodrop spectrophotometry. Linear amplification of 10 ng of total RNA was performed using the Ovation Biotin RNA amplification and labeling system (NuGEN). Fragmented, labeled cDNA was hybridized to Affymetrix U133 plus 2.0 arrays.

Single-cell RNA sequencing. *Sample processing.* All samples were processed within one hour from venipuncture.

Cell sorting. PBMCs were isolated from fresh whole blood using Ficoll-Paque Plus (GE Healthcare) density gradient centrifugation. For cell sorting, we used fluorochrome-labeled antibodies specific for CD3 (UCHT1), CD27 (M-T271) (BioLegend), CD4 (RPA-T4), CD19 (HIB19), IgD (IA6-2), CD127 (HIL-$7R^-$M21) (BD Biosciences), and CD8 (SCF121Thy2D3) (Beckman Coulter). $CD8^+IL7R^+$ ($CD8^+CD127^+$) and $CD8^+IL7R^-$ ($CD8^+CD127^-$) T cells were sorted from the $CD19^-CD3^+CD4^-$ fraction. Cell sorting was performed using the FACSAria Fusion (BD Biosciences).

Blood preparation for single-cell RNA sequencing. PBMCs were thawed quickly at 37 °C and were transferred to Dulbecco's Modified Eagle's Medium supplemented with 10% fetal bovine serum. Cells were centrifuged at 400*g*, for 10 min. Cells were washed once with 1× PBS supplemented with 0.04% BSA and were finally resuspended in 1× PBS with 0.04% BSA. Viability was determined using trypan blue staining and measurement on a Countess FLII automated cell counter, and samples with <80% viability were discarded. A total of 12,000 cells was loaded for capture onto the Chromium System using the v2 single-cell reagent kit (10X Genomics). Following capture and lysis, cDNA was synthesized and amplified (12 cycles) according to the manufacturer's protocol (10X Genomics). The amplified cDNA was used to construct an Illumina sequencing library and was sequenced on a single lane of a HiSeq 4000 sequencing system (Illumina).

Single-cell raw data processing and data combination. Illumina basecall files (*.bcl) were converted to FASTQ files using cellranger v2.1.0, which uses bcl2fastq v2.17.1.14. FASTQ files were then aligned to the hg19 reference genome and reference transcriptome using the cellranger v2.1.0 pipeline, which generates a gene–cell expression matrix. The samples were merged together using the cellranger aggr pipeline from cellranger, which aggregates outputs from multiple runs, normalizing them to the same sequencing depth (normalize = mapped) and then recomputing the gene–barcode matrices; analysis is then carried out on the combined data (scripts are available at https://github.com/dnehar/Temra-IL7R-Senescence).

Scrublet for multiplet prediction and removal. Generally, we expected about 2–8% of the cells to be hybrid transcriptomes or multiplets, occurring when 2 or more cells are captured within the same microfluidic droplet and are tagged with the same barcode. Such artifactual multiplets can confound downstream analyses. We applied the Scrublet[45] Python package to remove the putative multiplets. Scrublet assigns each measured transcriptome a 'multiplet score', which indicates the probability of being a hybrid transcriptome. Multiplet scores were determined for each individual (using the raw data), and 0.7–10.7% of the highest scoring cells were tagged as multiplets after visual inspection of doublet score distributions, and were excluded from further analysis.

Single-cell processing, clustering and cell type classification. The aggregated matrices were fed into the Python-based Scanpy[46] workflow (https://scanpy.readthedocs.io/en/stable), which includes preprocessing, visualization, clustering and differential expression testing. The pipeline we used was inspired by the Seurat[47] R package workflow.

Quality control and cell filtering. We applied the following filtering parameters: 1) all genes that were not detected in ≥3 cells were discarded, 2) cells with less than 400 total unique transcripts were removed prior to downstream analysis, 3) cells in which >20% of the transcripts that mapped to the mitochondrial genes were filtered out, as this can be a marker of poor-quality cells and 4) cells displaying a unique gene count of >2,500 genes were considered to be outliers and were discarded.

Data normalization. After discarding unwanted cells from the data set, we normalized the data. Library-size normalization was performed on the basis of gene expression for each barcode by scaling the total number of transcripts per cell to 10,000. We log-transformed the data and then regressed out using the total number of genes and the fraction of mitochondrial transcript content per cell. Then, 1,202 highly variable genes were identified using the filter_genes_dispersion Scanpy function and were used to perform the principal component analysis.

Linear dimensional reduction using principal component analysis and graph-based clustering. Dimensionality reduction was carried out in Scanpy via principal component analysis followed by Louvain clustering UMAP visualization using the top 40 significant components (principal components)[48].

Finding marker genes and evaluation of cluster identity. To annotate the cell type of each single-cell transcriptome, we used both differential expression analysis between clusters and classification based on putative marker gene expression. We applied the 'tl.rank_genes_groups' Scanpy function to perform differential analyses, and compared each cluster to the rest of the cell using the Wilcoxon test (Supplementary Table 3). We only considered clusters that showed a distinct trancriptomic program.

Batch effect correction. We performed a batch (10X genomics batch) correction using BBKNN (https://github.com/Teichlab/bbknn)[49]. More details about the parameters used can be found as a Jupyter notebook at https://github.com/dnehar/Temra-IL7R-Senescence.

NK and senescence scores. Gene lists (Supplementary Table 3) were used to score NK or senescence expression in naive and T_{EMRA} $CD8^+$ T cells. To do so, we calculated the mean expression for each cell, within each cluster using the h5ad object (adata), as follows:

adata.obs['NK_score'] = adata.X[:,NK_markers].mean(1).

The scores were then plotted, as shown in Fig. 3d.

Lentiviral transduction. Sestrin knockdown in human $CD8^+$ T cells was achieved using a lentiviral transduction system as described previously[9].

The pHIV1-SIREN-GFP system used for knockdown of gene expression possesses a U6-shRNA cassette to drive shRNA expression and a GFP reporter gene that is controlled by a PGK promoter. The following siRNA sequences were used for gene knockdowns: CCTAAGGTTAAGTCGCCCTCG (shCTRL), CCAGGACCAATGGTAGACAAA (shSesn1), CCGAAGAATGTACAACCTCTT (shSesn2) and CAGTTCTCTAGTGTCAAAGTT (shSesn3). VSV-g pseudotyped lentiviral particles were produced, concentrated and titrated in HEK293 cells as described[9].

Cells were cultured in RPMI-1640 medium supplemented with 10% heat-inactivated FCS, 100 U ml^{-1} penicillin, 100 mg ml^{-1} streptomycin, 50 μg ml^{-1} gentamicin, 2 mM L-glutamine (all from Invitrogen) and 0.5 ng ml^{-1} anti-mycoplasma (Bio-Rad) at 37 °C in a humidified 5% CO_2 incubator. Purified human

highly differentiated CD28$^-$CD8$^+$ T cells were activated in the presence of plate-bound anti-CD3 (purified OKT3, 0.5 µg ml^{-1}) plus rhIL-2 (R&D Systems, 10 ng ml^{-1}), and then transduced with pHIV1-Siren lentiviral particles (multiplicity of infection = 10) 72 h after activation.

Flow cytometry and phospho-flow. Multi-parameter flow cytometry was used for phenotypic and functional analyses of PBMCs. For analysis of surface markers, staining was performed at 4 °C for 30 min in the presence of saturating concentrations of antibodies (listed in Supplementary Table 5) and a live/dead fixable Near-Infrared stain (Thermo Fisher Scientific, L10119). For intracellular analysis of cytokine secretion, cytotoxic granule expression, and sestrin 1, sestrin 2, DAP12, and DAP10 expression, cells were fixed and permeabilized with the Fix & Perm Kit (Invitrogen, Life Technologies), before incubation with indicated antibodies or the respective isotype controls. For imaging cytometry, samples were acquired on an Amnis ImageStreamX MkII (Luminex) using INSPIRE software, magnification ×60. Data were analyzed using Amnis IDEAS v6.2 software (Luminex). Colocalization of signals was determined on a single-cell basis using bright detail similarity (BDS) score analysis. Colocalization was considered with BDS ≥ 2.0.

For phospho-flow cytometry, after staining for surface markers, CD8$^+$ T cells were stimulated with anti-CD3 (purified OKT3, 10 µg ml^{-1}) for 30 min on ice, followed by crosslinking with goat anti–mouse IgG antibody during 30 min on ice. Cells were then transferred to an incubator at 37 °C, and stimulation was terminated after 10 min, with immediate fixation with Cytofix Buffer (PBS containing 4% paraformaldehyde, BD Biosciences) followed by permeabilization with ice-cold Perm Buffer III (PBS containing 90% methanol, BD Biosciences) and staining with antibodies for phosphoproteins (listed in Supplementary Table 5) for 30 min at room temperature. Samples were acquired on an LSR II flow cytometer (BD Biosciences) and were analyzed using FlowJo software (TreeStar).

Cytotoxic assays - CD107a degranulation assay. Freshly isolated NK and CD8$^+$ T cell subsets were incubated at 37 °C for 6 h with K562 or C1R–MICA/C1R cells, at a fixed E:T ratio of 2:1, in the presence of APC-conjugated CD107a antibody (BD Biosciences), as previously described[21]. Brefeldin A (1 µg ml^{-1}, Sigma-Aldrich) and Monensin (1 µg ml^{-1}, Sigma-Aldrich) were added in the final 5 h incubation period. Effector cells incubated alone in the presence of phorbol-12-myristate-13-acetate (PMA, 50 ng ml^{-1}, Sigma-Aldrich) with ionomycin, (250 ng ml^{-1}, Sigma-Aldrich) were used as a positive control whereas medium alone served as an unstimulated control. After incubation, cells were stained for surface markers for 30 min on ice, followed by intracellular detection of cytokines (TNF-α and IFN-γ) and CD107a expression, and were analyzed by flow cytometry.

Cell lines. The K562 (human erythroleukemic) cell line was purchased from the European Collection of Authenticated Cell Cultures (ECCAC) and was cultured in 25 cm^2 flasks (Nunc) in complete RPMI-1640 medium. B-lymphoblastoid cell lines, C1R and C1R transfected with MICA*008 (C1R–MICA) were kindly provided by A. Toubert (INSERM UMR1160, Paris) and were maintained in complete RPMI-1640 in the presence of the aminoglycoside antibiotic G-418 (Sigma, G8168) for selection of transfected cells[50].

Immunoblotting. Human CD8$^+$ T cell subsets purified using immunomagnetic separation (MACS) according to CD27/CD28 expression were stimulated with anti-CD3 (purified OKT3, 10 µg ml^{-1}) or anti-NKG2D (1D11, 10 µg ml^{-1}) before lysis. Cells were normalized by equal cell number, harvested and lysed in ice-cold radioimmunoprecipitation assay (RIPA) buffer (Sigma-Aldrich), supplemented with protease and phosphatase inhibitors (GE Healthcare), for 30 min on ice. Cell lysates were processed for immunoblot analysis as described[6].

Immunoprecipitation. Human CD8$^+$ T cells were separated into CD28$^+$/CD28$^-$ fractions (to obtain sufficient numbers of cells for analysis) and stimulated with anti-NKG2D (1D11, 10 µg ml^{-1}) or isotype control, for 30 min at 4 °C. Lysates from 1×10^7 cells were prepared with ice-cold HNGT buffer (50 mM HEPES, pH 7.5, 150 mM EDTA, 10 mM sodium pyrophosphate, 100 mM sodium orthovanadate, 100 mM sodium fluoride, 10 mg ml^{-1} aprotinin, 10 mg ml^{-1} leupeptin and 1 mM phenylmethylsulfonyl fluoride), for 30 min on ice. Cell lysates were incubated overnight at 4 °C with anti-NK2D antibody (clone Santa Cruz, 5C6) or control antibody, followed by precipitation with 10 µl of prewashed protein A/G agarose beads (Santa Cruz, sc-2003) for 3 h at 4 °C on a rotary shaker. After extensive washing in HGNT buffer, supernatants were recovered and processed for immunoblot analysis, as described above. Coimmunoprecipitated proteins were detected after incubation with primary antibodies followed by incubation with mouse anti–rabbit IgG (conformation-specific antibody; Cell Signaling Technology, L27A9) or mouse anti–rabbit IgG light chain (Cell Signaling Technology, L57A3) and by a secondary anti–mouse IgG antibody (Cell Signaling Technology, 7076).

Mice. *Sesn1*$^{-/-}$ and *Sesn2*$^{-/-}$ mice were described previously[7]. The mouse aging study was performed at the University of Michigan, where the animal procedures were approved by the Institutional Animal Care & Use Committee and were overseen by the Unit for Laboratory Animal Medicine. All mice were rested for at least 10 d before being used for in vivo studies. Animals were housed under standard conditions, maintained in a 12 h/12 h light/dark cycle at 22 °C ± 1 °C and were given food and tap water ad libitum in accordance with United Kingdom Home Office regulations (PPL-P69E3 D849) and the National Institutes of Health guidelines.

Murine delayed-type hypersensitivity model. Knockout and age-matched (18-month-old) C57BL/6J WT control mice were imported from the University of Michigan. Young (~6 weeks) WT mice were purchased separately from Charles River. All mice were male. The mBSA DTH model was performed as described previously[51]. Mice were sensitized at the base of the tail with a 50 µl injection of mBSA in Freund's complete adjuvant (20 mg ml^{-1} solution of mBSA in saline emulsified with an equal volume of Freund's adjuvant containing 4 mg ml^{-1} *Mycobacterium tuberculosis* strain H37Ra, Sigma-Aldrich). An immune response was evoked 14 d later by subplantar challenge with 50 µl of mBSA in saline (1 mg ml^{-1}). The contralateral paw received a saline-only injection and served as a control. The immune response is reported as the difference in paw swelling between left and right paws as determined using calipers (POCO2, Kroeplin). Mice were killed 7 days post challenge, according to Schedule 1, using an increasing concentration of CO_2. Death was confirmed by cervical dislocation. Spleens and inguinal lymph nodes were obtained, weighed and dispersed through a 70 µm, followed by a 35 µm, sterile cell sieve (Becton Dickinson) to yield single-cell suspensions. Cell numbers were enumerated by haemocytometer and up to 10^6 cells were used for polychromatic flow cytometry.

In vivo cytotoxicity. Twenty-four-month-old knockout (*Sesn1*$^{-/-}$; *Sesn2*$^{-/-}$; *Sesn3*$^{+/-}$) male mice were imported from the University of Michigan. Age-matched WT female C57Bl/6J mice were purchased from Envigo. NK cells were depleted by intraperitoneal injection of 100 µg anti-NK1.1 antibody (Bio X Cell, PK136) 24 h before cell challenge. The myeloma cell line 5TGM, which expresses high levels of Rae-1, was labeled with 5 µM carboxyfluorescein succinimidyl ester (CFSE), whereas splenocytes stained with 0.5 µM were used as Rae-1$^-$ controls. Both cell types were mixed at equal ratios and 2×10^7 cells were coinjected intravenously. Mice were left for 6 h before being killed. As a measure of Rae-1-directed killing, the ratio of CFSE^{hi} compared to CFSE^{lo} was used to determine Rae-1$^+$ cell retrieval and specific lysis.

Statistical analysis. Statistical analysis was performed using GraphPad Prism version 6.00. Tests were used to determine data distribution and depending on the normality of the data, comparisons were performed using the Student *t* test (for two groups, parametric) or the non-parametric Mann–Whitney U test (for two groups, unpaired) and the Wilcoxon signed rank test (for two groups, paired) with two-tailed *P* values unless otherwise stated. When comparing more than 2 groups, we used one-way ANOVA (parametric, >2 groups, unpaired), repeated measures ANOVA (parametric, >2 groups, paired), Kruskal–Wallis (non-parametric, >2 groups, unpaired) or Friedman (non-parametric, >2 groups, paired) tests with post-correction for multiple comparisons, as appropriate. The two-way ANOVA test was used to compare the effects of two independent variables between groups. Linear regression analysis was performed to generate lines of best fit and correlations between variables were analyzed using Pearson´s or Spearman's rank correlation coefficient (*r*). Differences were considered to be significant when $P < 0.05$ (*), $P < 0.01$ (**), $P < 0.001$ (***) and $P < 0.0001$ (****). Data are presented as means ± s.e.m. unless otherwise stated.

Reporting Summary. Further information on research design is available in the Nature Research Reporting Summary linked to this article.

Data availability

The data that support the findings of this study are available from the corresponding author upon request. The complete microarray data set is available online from the NCBI Gene Expression Omnibus public repository (GEO accession number GSE98640). The scRNA-seq data are available on EGA (accession number EGAS00001004255).

References

42. Ucar, D et al. The chromatin accessibility signature of human immune aging stems from CD8$^+$ T cells. *J. Exp. Med.* **214**, 3123–3144 (2017).
43. Callender, L. A. et al. Human CD8$^+$ EMRA T cells display a senescence-associated secretory phenotype regulated by p38 MAPK. *Aging Cell* **17**, e12675 (2018).
44. Gérart, S. et al. Human iNKT and MAIT cells exhibit a PLZF-dependent proapoptotic propensity that is counterbalanced by XIAP. *Blood* **121**, 614–623 (2013).
45. Wolock, S. L., Lopez, R. & Klein, A. M. Scrublet: computational identification of cell doublets in single-cell transcriptomic data. *Cell Syst.* **8**, 281–291.e9 (2019).
46. Wolf, F. A., Angerer, P. & Theis, F. J. SCANPY: large-scale single-cell gene expression data analysis. *Genome Biol.* **19**, 15 (2018).

47. Satija, R., Farrell, J. A., Gennert, D., Schier, A. F. & Regev, A. Spatial reconstruction of single-cell gene expression data. *Nat. Biotechnol.* **33**, 495–502 (2015).
48. McInnes, L., Healy, J. & Melville, J. UMAP: uniform manifold approximation and projection for dimension reduction. Preprint at *aRxiv* https://arxiv.org/abs/1802.03426v2 (2018).
49. Polański, K et al. Fast batch alignment of single cell transcriptomes unifies multiple mouse cell atlases into an integrated landscape. *Bioinformatics* **36**, 964–965 (2020).
50. Allez, M. et al. $CD4^+NKG2D^+$ T cells in Crohn's disease mediate inflammatory and cytotoxic responses through MICA interactions. *Gastroenterology* **132**, 2346–2358 (2007).
51. Trivedi, S. G. et al. Essential role for hematopoietic prostaglandin D2 synthase in the control of delayed type hypersensitivity. *Proc. Natl Acad. Sci. USA* **103**, 5179–5184 (2006).

Acknowledgements

We thank A. Toubert from INSERM U.1160 and Laboratoire d´Immunologie et d´Histocompatibilité, Hôpital Saint-Louis, Université Paris Diderot, Sorbonne Paris Cité for the kind gift of the $C1R^{-}$MICA cell line. B.I.P. was supported by the Portuguese Foundation for Science and Technology and the Gulbenkian Institute for Science sponsoring the Advanced Medical Program for Physicians (PFMA). This work was supported by the Medical Research Council (grant MR/P00184X/1 to A.N.A.), the Ministry of Education of Brazil (grant BEX9414/14-2 to L.P.C.), the Wellcome Trust (grant AZR00630 to A. Lanna), University College London Business (to S.M.H. and A.N.A. for the microarray work), the National Institutes of Health (R01DK102850 and R01DK111465 to J.H.L.), the NIH/NIAID (R01 AG052608 and R01 AI142086 to J.B.) and the Biotechnology and Biological Science Research Council (grant BB/L005336/1 to N.E.R.). R.P.H.D was supported, in part, by the NIHR UCL Hospital Biomedical Research Centre, and S.M.H. is funded by the Springboard award from the Academy of Medical Science and the Wellcome Trust. A.L. is a Sir Henry Wellcome Trust Fellow sponsored by M. L. Dustin (University of Oxford). S.M.J. is a Wellcome Trust Senior Fellow in Clinical Science and is supported by the Rosetrees Trust, the Welton Trust, the Garfield Weston Trust and the UCLH Charitable Foundation. S.M.J. and V.H.T. have been funded by the Roy Castle Lung Cancer Foundation. D.U. is supported by the National Institute of General Medical Sciences (NIGMS) under award number GM124922. G.A.K. is supported by the Travelers Chair in Geriatrics and Gerontology, as well as the National Institute on Aging (AG061456, AG048023, AG063528, AG060746, AG021600, AG052608 and AG051647).

Author contributions

B.I.P., L.P.C and R.P.H.D. designed and performed the experiments, analyzed the data and wrote the manuscript. D.N.-B. designed and analyzed the scRNA-seq data under the supervision of J.B. and D.U. R.M. performed all the experiments with the healthy older adult subjects. G.A.K. recruited all the healthy older adult donor subjects in Farmington, CT. A. Lanna, E.S.C. and N.E.R. designed and performed experiments. S.W. and J.S. designed and performed in vivo cytotoxicity studies. S.M.H. and A.N.A. designed and performed the microarray studies. A. Larbi provided support for studies of NKR on T cells. N.A.M., V.H.T. and S.M.J. analyzed the microarray and RNA-seq data. D.C.O.G., D.W.G., J.H.L. and M.K.M. facilitated mouse experiments. A.N.A. designed the experiments, reviewed and edited the manuscript, and organized the collaborative infrastructure.

Competing interests

The authors declare no competing interests.

Additional information

Extended data is available for this paper at https://doi.org/10.1038/s41590-020-0643-3.

Supplementary information is available for this paper at https://doi.org/10.1038/s41590-020-0643-3.

Correspondence and requests for materials should be addressed to A.N.A.

Peer review information Ioana Visan was the primary editor on this article and managed its editorial process and peer review in collaboration with the rest of the editorial team.

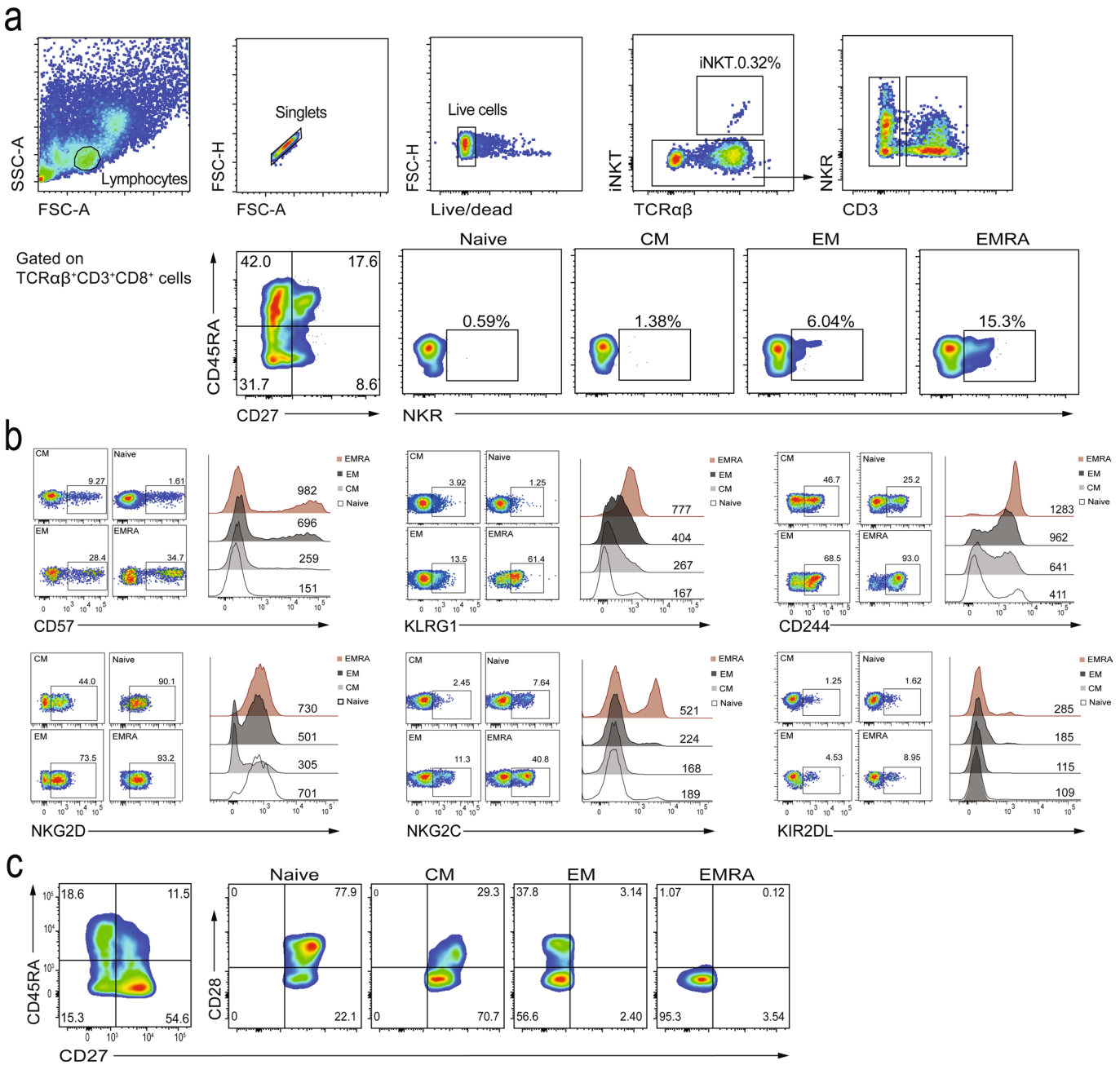

Extended Data Fig. 1 | CD^{8+} T cell gating and NKR expression. a, Representative flow cytometry plots showing T cell gating and NKR expression on peripheral blood lymphocytes, specifically focusing on CD8$^+$ T cell subsets stratified by the expression of CD27/CD45RA in healthy donors. Defined subsets are CD27$^+$CD45RA$^+$ T_N, CD27$^+$CD45RA$^-$ T_{CM}, CD27$^-$CD45RA$^-$ T_{EM}, and CD27$^-$CD45RA$^+$ T_{EMRA} cells. **b**, Confirmation of expression of CD57, KLRG1, CD244, NKG2D, NKG2C, and KIR2DL on T_N (naive), T_{CM}, T_{EM}, and T_{EMRA} CD8$^+$ T cell subsets. Numbers in quadrants represent percentages of cells in each subset. Numbers above the histograms indicate the MFI. **c**, Flow cytometry gating of CD8$^+$ T cells to confirm CD27 and CD28 expression in subpopulations based on CD27/CD45RA gating.

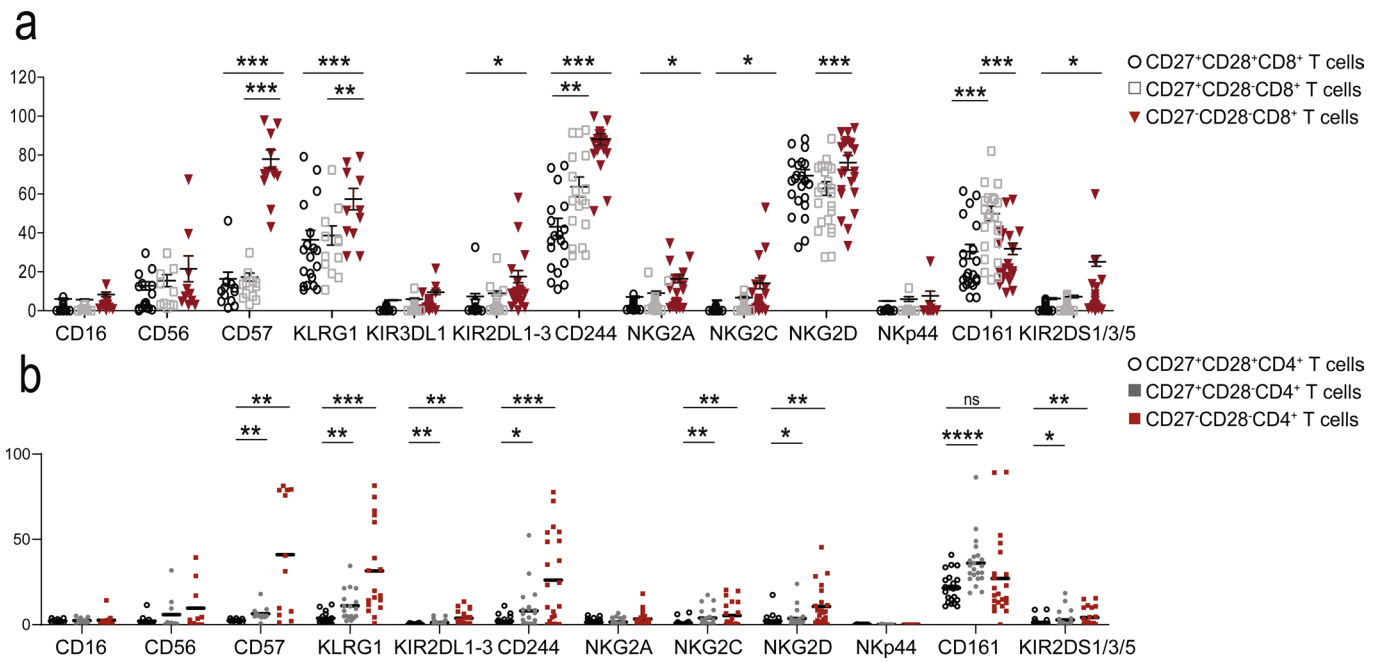

Extended Data Fig. 2 | NKR expression in CD8⁺ and CD4⁺ T cells defined by CD27/CD28. Expression of NK cell receptors (NKR) on **a**, CD8⁺ and **b**, CD4⁺ T cells assessed by flow cytometry on PBMCs from 22 healthy donors (median age = 52, range 25-83). Total CD8⁺ and CD4⁺ T cells were stratified into three subsets according to CD27/CD28 expression as shown in Extended Data Fig. 1a.

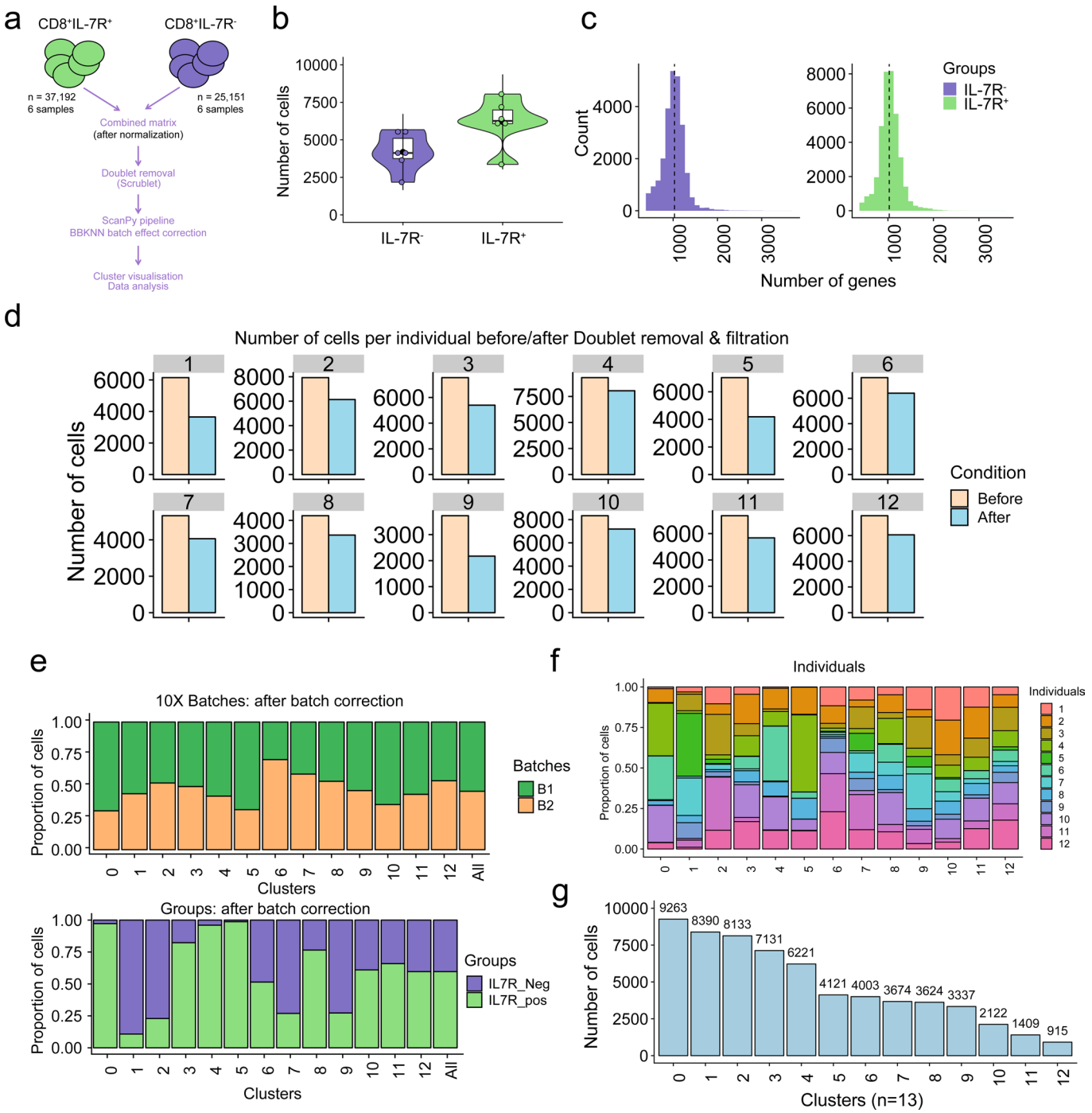

Extended Data Fig. 3 | scRNA-seq method and quality control. a, Overview of the scRNA-seq processing pipeline. Raw data (n=82,061 sorted CD8+ T cells) from six healthy older adult donors (six IL7R+ and six IL7R⁻ CD8+ T cell samples) were first cleaned from the multiplets, using Scrublet36, then merged, resulting in a data set containing 62,343 cells. After batch correction using BBKNN37, the Scanpy66 -based pipeline was ran (see Methods section). **b**, Number of cells per individual (n=12). IL7R+ (n=6, in green) and IL7R- (n=6; in purple). **c**, Number of genes per distribution across the IL7R+ (in green) and IL7R- (in purple) cells. **d**, Number of cells before (light orange) and after (light blue) filtration (that is, doublet removal and other filtration steps that are described in Methods), within each individual. **e**, Bar plot highlighting the cell abundances across clusters (n = 13) for 10X run batches (upper panel) and IL7R⁺ and IL7R⁻ groups (lower panel) after BBKNN batch effect correction. **f**, Bar plot highlighting the individual (n=12) cell abundances across clusters (n = 13) after BBKNN batch effect correction. Each color represents an individual. **g**, Number of cells in each cluster.

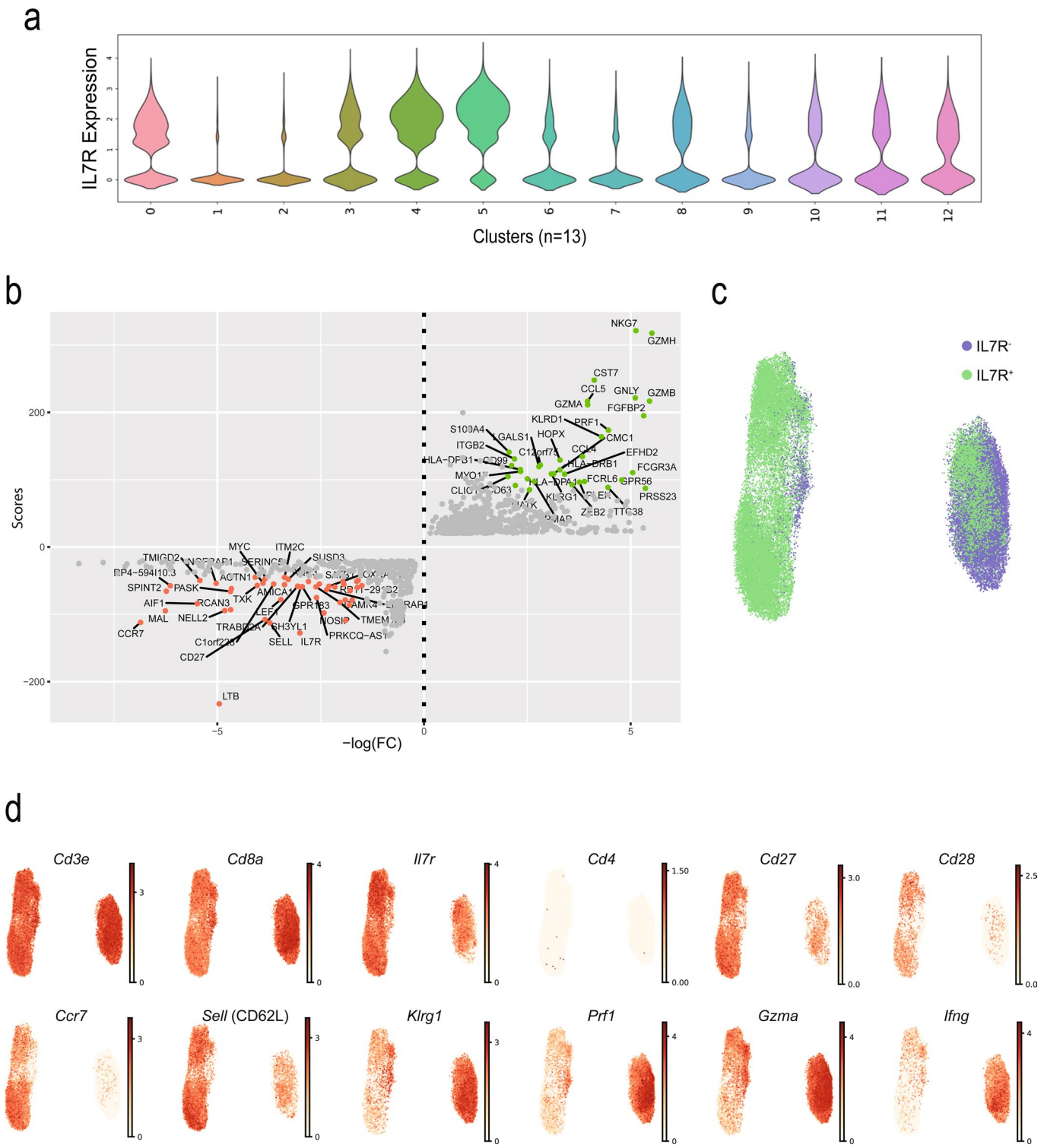

Extended Data Fig. 4 | scRNA-seq comparison of re-clustered CD8⁺ T cells. a, Violin plot showing the IL7R expression (as defined by scRNA-seq) across the 13 clusters. **b**, Dotplot showing the genes that are modulated in T_N (top genes in red) and T_{EMRA} (top genes in green) compartments. The scores (y axis) were defined using the Scanpy function (sc.tl.rank_genes_groups), based on Wilcoxon statistical test. FC = Fold change. T_N (C0, C4 and C8) and T_{EMRA} (C1, C2 and C6) compartments were extracted, a second round of clustering on the selected clusters (n = 39,634) was performed (as in Fig. 3) and UMAP plots highlighting **c**, *IL7R* groups (*IL7R*⁺ in green, *IL7R*⁻ in purple, as defined by flow sorting) and **d**, of representative genes are shown.

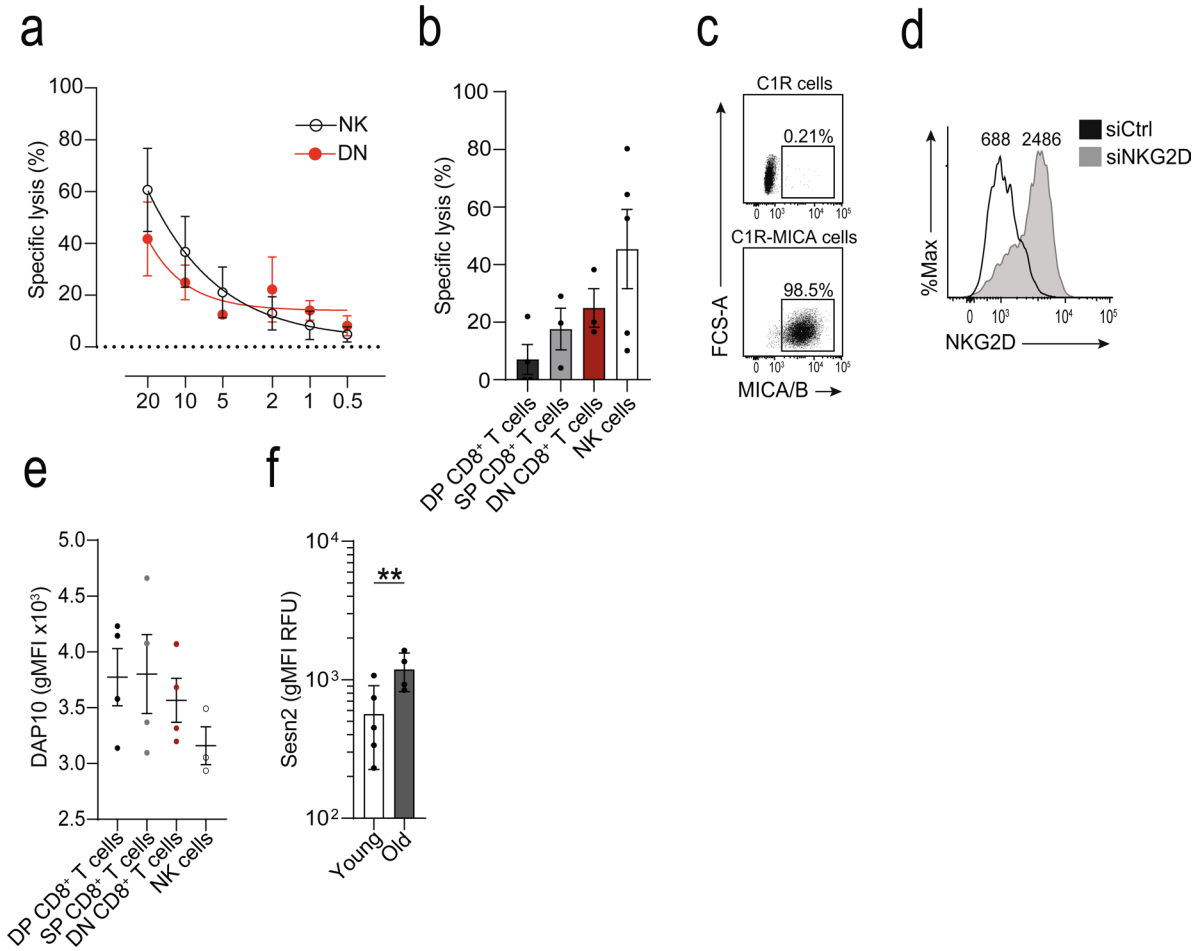

Extended Data Fig. 5 | Extended data on cytotoxicity and Sesn2 expression. a, Titration curve of varying effector to target (E:T) ratios on cytotoxicity measured as specific lysis of K562 cells using a calcein-release of $CD27^{-}CD28^{-}CD8^{+}$ (DN) T cells and NK cells isolated by FACS. Non-linear regression (5-parameter asymmetric) was performed (means and s.d., n = 3 donors). **b**, Calcein-release cytotoxicity assay of K562 cells by $CD27^{+}CD28^{+}$ (DP), $CD27^{+}CD28^{-}$ (SP), DN $CD8^{+}$ T cells, and NK cells at E:T 20:1. Cytotoxicity was assessed over a period of six hours (means and s.d., n = 3 donors). **c**, Representative dot plot of MICA/B expression in C1R and C1R-MICA*008 cells. **d**, Representative histogram of NKG2D expression on $CD28^{-}CD8^{+}$ T cells after transfection with NKG2D siRNA (siNKG2D, black) or scrambled siRNA (siCtrl, gray), determined 36 hours after transfection. Numbers indicate MFI. **e**, Expression of DAP10 on human NK cells, and DP, SP, and DN $CD8^{+}$ T cell subsets. Mean fluorescence intensity is shown (means and s.d., n = 4 for T cell, n = 3 NK cells). **f**, Sestrin 2 on $CD8^{+}$ T cells from young (<35 years, n = 5) and old (>65 years, n = 4) donors. MFIs are shown (geometric means and geometric s.d. factor). Two-tailed, unpaired Welch's t-test, ** $p < 0.01$.

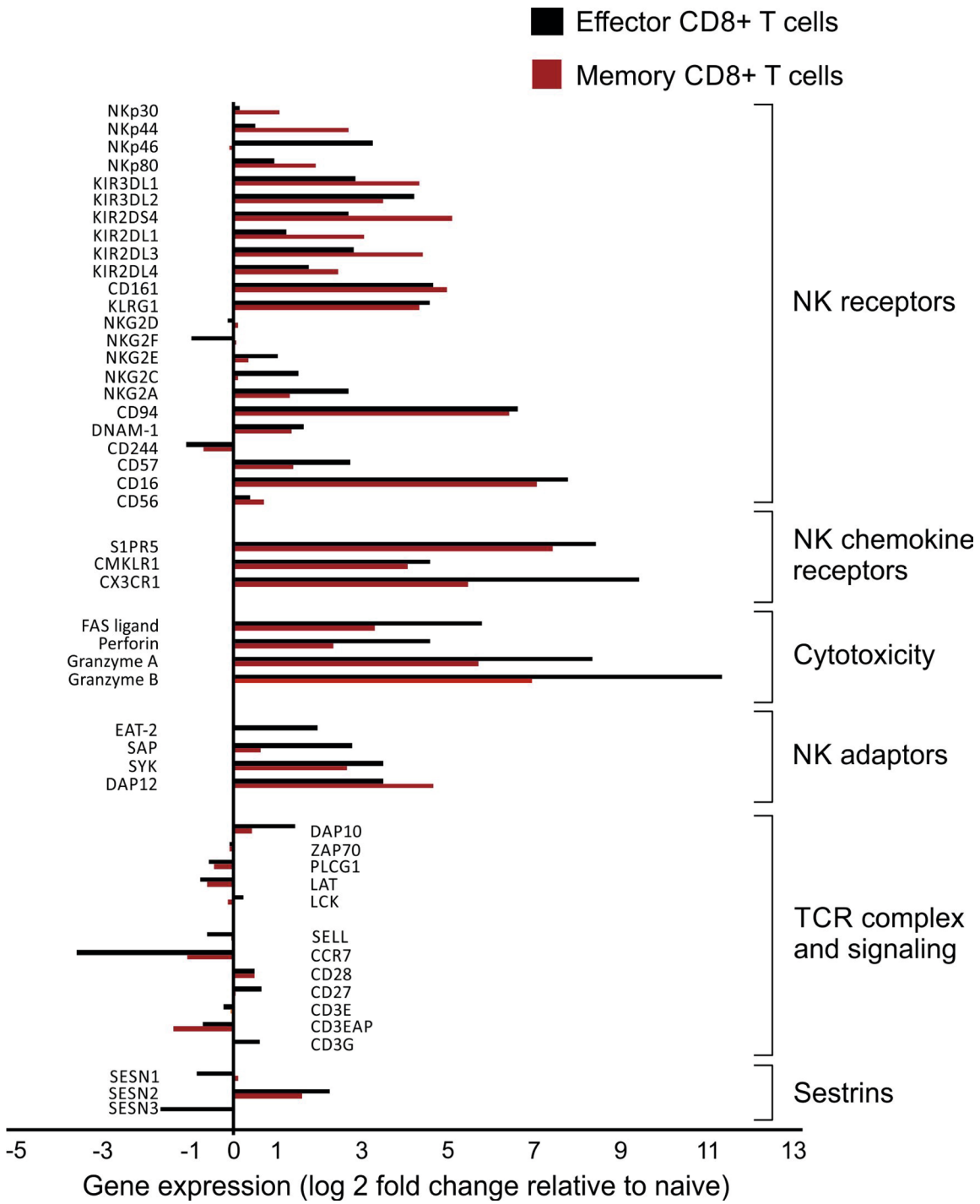

Extended Data Fig. 6 | YFV-tet$^+$CD8$^+$ T cells exhibit an NK phenotype. Data mined from Akondy *et al.* (GSE100745)[28] showing the relative fold change (log_2) of differentially expressed genes of interest in YFV-tetramer$^+$ effector (14 days post vaccination, black bars, n = 3) or memory (4–12 years post vaccination, red bars, n = 5) compared to naive (n = 6) CD8$^+$ T cells.

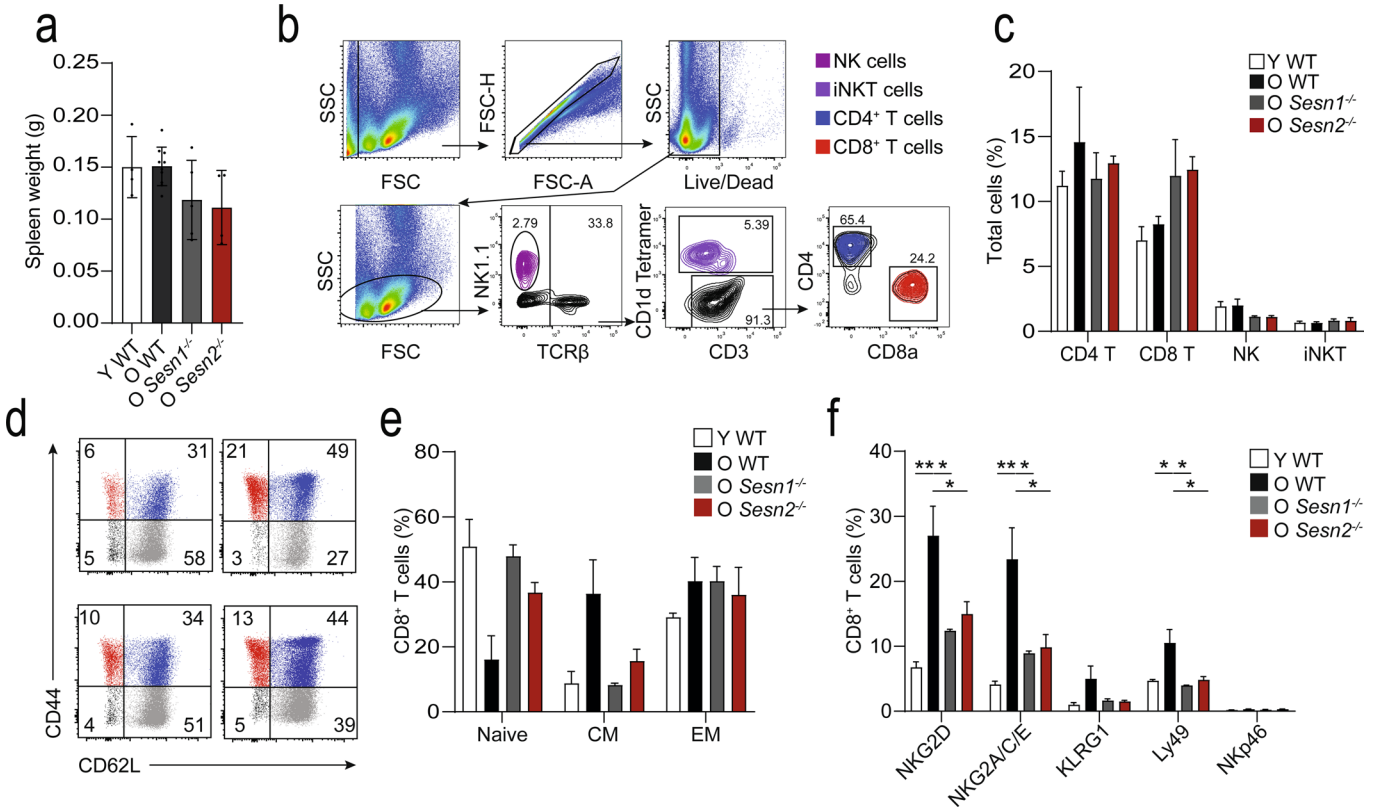

Extended Data Fig. 7 | Extended data on the murine delayed-type hypersensitivity model. a, Spleen weight following mBSA-driven DTH response in young WT (Y WT, n = 4 mice), old WT (O WT, n = 8 mice), old *Sesn1*$^{-/-}$ (O *Sesn1*$^{-/-}$, n = 5 mice), and old *Sesn2*$^{-/-}$ (O *Sesn2*$^{-/-}$, n = 4 mice). Bars represent means and s.d.. **b**, Representative gating strategy to identify NK1.1^{+} NK cells (violet), TCRβ^{+}CD1d tetramer reactive iNKT cells (purple), TCRβ^{+}CD3^{+} CD4^{+} (blue) and CD8^{+} (red) T cells in mice. Similar results were obtained in all mice (n = 3 per group). **c**, Quantification of these cell types in the spleen (means and s.e.m., n = 3 mice per group). **d**, Dot plots showing relative frequencies of CD44^{-}CD62L^{+} naive (gray), CD44^{+}CD62L^{+} central (blue), and CD44^{+}CD62L^{-} effector (red) CD8^{+} T cells. **e**, Quantification of these cell types as a proportion of total splenic CD8^{+} T cells (means and s.e.m., n = 3 per group). **f**, Enumeration of NKG2D, NKG2A/C/E, KLRG1, Ly49, and NKp46 expression on CD8^{+} T cells from Y WT, O WT, O *Sesn1*$^{-/-}$, and O *Sesn2*$^{-/-}$ mice (means and s.e.m., n = 3 per group). One-way ANOVA with Tukey's multiple comparisons test. * $p < 0.05$, ** $p < 0.01$, *** $p < 0.001$, **** $p < 0.0001$.

nature research

Corresponding author(s): Arne N Akbar

Last updated by author(s): Feb 21, 2020

Reporting Summary

Nature Research wishes to improve the reproducibility of the work that we publish. This form provides structure for consistency and transparency in reporting. For further information on Nature Research policies, see Authors & Referees and the Editorial Policy Checklist.

Statistics

For all statistical analyses, confirm that the following items are present in the figure legend, table legend, main text, or Methods section.

n/a	Confirmed	
☐	☒	The exact sample size (*n*) for each experimental group/condition, given as a discrete number and unit of measurement
☐	☒	A statement on whether measurements were taken from distinct samples or whether the same sample was measured repeatedly
☐	☒	The statistical test(s) used AND whether they are one- or two-sided *Only common tests should be described solely by name; describe more complex techniques in the Methods section.*
☐	☒	A description of all covariates tested
☐	☒	A description of any assumptions or corrections, such as tests of normality and adjustment for multiple comparisons
☐	☒	A full description of the statistical parameters including central tendency (e.g. means) or other basic estimates (e.g. regression coefficient) AND variation (e.g. standard deviation) or associated estimates of uncertainty (e.g. confidence intervals)
☐	☒	For null hypothesis testing, the test statistic (e.g. *F*, *t*, *r*) with confidence intervals, effect sizes, degrees of freedom and *P* value noted *Give P values as exact values whenever suitable.*
☒	☐	For Bayesian analysis, information on the choice of priors and Markov chain Monte Carlo settings
☒	☐	For hierarchical and complex designs, identification of the appropriate level for tests and full reporting of outcomes
☒	☐	Estimates of effect sizes (e.g. Cohen's *d*, Pearson's *r*), indicating how they were calculated

Our web collection on statistics for biologists contains articles on many of the points above.

Software and code

Policy information about availability of computer code

Data collection	BD FACSDiva v8.0.3, INSPIRE v200.0.482, Zen Blue v2.3, MxPro QPCR v4.1D, CLARIOstar Reader Control Software v5.61
Data analysis	Microsoft Excel (Outlook 365), GraphPad Prism v8.0.1, FlowJo v10.5.3, ImageJ v2.0.0-rc-69/1, IDEAS v6.2, cellranger v2.1.0, bcl2fastq v2.17.1.14, ScanPy v1.4.4.post1, anndata v0.6.22.post1, umap v0.3.10, numpy v1.17.2, scipy v1.3.1, pandas v0.25.1 scikit-learn v0.21.3 statsmodels v0.10.1, python-igraph v0.7.1, louvain v0.6.1 Script used for the analysis (and the versions) can be found here: https://github.com/dnehar/Temra-IL7R-Senescence

For manuscripts utilizing custom algorithms or software that are central to the research but not yet described in published literature, software must be made available to editors/reviewers. We strongly encourage code deposition in a community repository (e.g. GitHub). See the Nature Research guidelines for submitting code & software for further information.

Data

Policy information about availability of data

All manuscripts must include a data availability statement. This statement should provide the following information, where applicable:

- Accession codes, unique identifiers, or web links for publicly available datasets
- A list of figures that have associated raw data
- A description of any restrictions on data availability

The authors declare that the data supporting the findings of this study are available within the paper and its supplementary information files. Any raw data relevant to this study are available from the corresponding author upon reasonable request.

Field-specific reporting

Please select the one below that is the best fit for your research. If you are not sure, read the appropriate sections before making your selection.

☒ Life sciences ☐ Behavioural & social sciences ☐ Ecological, evolutionary & environmental sciences

For a reference copy of the document with all sections, see nature.com/documents/nr-reporting-summary-flat.pdf

Life sciences study design

All studies must disclose on these points even when the disclosure is negative.

Sample size	No power calculations were performed. Sample sizes for Sesn biochemistry were estimated based on previous published data (Lanna et al. 2017 Nat Immunol). Sample sizes for NKR expression were based on existing literature on CD8 T cell NKR expression, we based our final numbers (22 donors) on the need to detect significant differences ($p < 0.05$) bearing in mind multiple comparisons. Sample sizes for mouse experiments were again based on previous literature and availability of rare sestrin knockout mice of advanced age.
Data exclusions	Some scRNA-seq samples were excluded based on QC explained in details in methods.
Replication	All protein analysis (flow cytometry and Western blots) were performed by 2-3 independent researchers that could reproduce the data contained in the manuscript. Microarray analysis was performed only once, but scrutinized by two independent groups of researchers. Mouse experiments were performed once. Data analysis was performed by at least two separate researchers. Where experiments were replicated, similar results were obtained.
Randomization	There was no randomization of cohorts. Allocations were done based on age groups of participants in the parent study.
Blinding	The nature of the work with human research participants donating samples used in flow cytometry or similar analysis meant no blinding was performed. Investigators consented and collected blood samples from donors themselves. Flow cytometry gating and western blot densitometry is performed based on set parameters governed by controls, therefore unblinded analysis was kept as unbiased as possible. Blinding was performed wherever possible: murine experiments were blinded in a way where one investigator assigned codes to individual mice which were handled and analyzed by others. Samples were unblinded following final flow cytometry analysis.

Reporting for specific materials, systems and methods

We require information from authors about some types of materials, experimental systems and methods used in many studies. Here, indicate whether each material, system or method listed is relevant to your study. If you are not sure if a list item applies to your research, read the appropriate section before selecting a response.

Materials & experimental systems

n/a	Involved in the study
☐	☒ Antibodies
☐	☒ Eukaryotic cell lines
☒	☐ Palaeontology
☐	☒ Animals and other organisms
☐	☒ Human research participants
☒	☐ Clinical data

Methods

n/a	Involved in the study
☒	☐ ChIP-seq
☐	☒ Flow cytometry
☒	☐ MRI-based neuroimaging

Antibodies

Antibodies used	Please see supplementary table 5 in the paper for this information. Due to the extended nature of this study (spanning multiple years) more than one lot of antibodies was used for experiments. Similar results were obtained regardless.
Validation	All antibodies were used based on manufacturers' validation. All have been validated for use with human cells and for use in either flow cytometry, functional assays, immunoblotting or immunoprecipitation. We optimised concentrations of certain flow cytometry antibodies for use with human blood and blister samples by performing single stains alongside isotype controls. FMO controls were used for flow cytometry. Secondary only stains were used for histology samples. Concentrations for functional assays (anti-CD3, OKT3 and anti-NKG2D 1D11, were based on previous literature).

Eukaryotic cell lines

Policy information about cell lines

Cell line source(s)	K562 - Caltag Medsystems

Authentication	No cell lines were authenticated in house.
Mycoplasma contamination	Cells are routinely tested for mycoplasma and were only used when no contamination was detected.
Commonly misidentified lines (See ICLAC register)	We did not use any commonly misidentified cell lines.

Animals and other organisms

Policy information about studies involving animals; ARRIVE guidelines recommended for reporting animal research

Laboratory animals	Wild type C57BL/6J mice, males and females, 6 weeks old or 18-24 month old. Sesnl-/- and Sesn2-/- knockout mice are on a C57BL/6J background, males, 18 months old.
Wild animals	We did not use wild animals.
Field-collected samples	We did not collect samples in the field.
Ethics oversight	University of Michigan: animal husbandry and procedures were approved by the Institutional Animal Care & Use Committee in accordance with the NIH guideline. UCL: animal husbandry and procedures were all performed in accordance with the Animals (Scientific Procedures) Act under UK Home Office regulations (PPL-P69E3D849).

Note that full information on the approval of the study protocol must also be provided in the manuscript.

Human research participants

Policy information about studies involving human research participants

Population characteristics	A total of 50 healthy people (males and females) over the age of 18 (range 25-82, median age 52) were recruited into the study. These participants described themselves as healthy. No genotypic data were collected.
Recruitment	Donors did not fall within the exclusion criteria described in the paper. Donors did not have any co-morbidity, were not on immunosuppressive drugs, and retained physical mobility and lifestyle independence. Participants were recruited by investigators from an internally curated database of donors formed of people living in and around London. They all self-assessed as healthy.
Ethics oversight	These studies were approved by the UCL Research Ethics Committee (Ref: 11/0473). Written informed consent was obtained from all volunteers. The scRNA-seq study was approved by the Institutional Review Board of UConn Health Center.

Note that full information on the approval of the study protocol must also be provided in the manuscript.

Flow Cytometry

Plots

Confirm that:

☒ The axis labels state the marker and fluorochrome used (e.g. CD4-FITC).

☒ The axis scales are clearly visible. Include numbers along axes only for bottom left plot of group (a 'group' is an analysis of identical markers).

☒ All plots are contour plots with outliers or pseudocolor plots.

☒ A numerical value for number of cells or percentage (with statistics) is provided.

Methodology

Sample preparation	Multi-parameter flow cytometry was used for phenotypic and functional analyses of PBMC. For analysis of surface markers, staining was performed at 4°C for 30 min in the presence of saturating concentrations of antibodies (listed in Table 2) and a live/dead fixable Near-Infrared stain (Thermo Scientific, L10119). For intracellular analysis of cytokine secretion, cytotoxic granule expression, and sestrin 1, sestrin 2, DAP12, and DAP10 expression, cells were fixed and permeabilized with the Fix & Perm® Kit (Invitrogen, Life Technologies, UK), before incubation with indicated antibodies or the respective isotype controls. For imaging cytometry, samples were acquired on an Amnis ImageStreamX Mk2 using INSPIRE software, magnification 60X. Data were analysed using IDEAS v6.2 software (Amnis). Co-localization of signals was determined on a single cell basis using bright detail similarity (BDS) score analysis. Co-localization was considered with BDS ≥ 2.0. For Phospho-Flow cytometry, after staining for surface markers, CD8+ T cells were stimulated with anti-CD3 (purified OKT3, 10 µg/mL) for 30 minutes on ice, followed by crosslinking with goat anti–mouse IgG antibody during 30 minutes on ice. Cells were then transferred to an incubator at 37°C, and stimulation was terminated after 10 minutes, with immediate fixation with Cytofix Buffer (PBS containing 4% paraformaldehyde, BD Biosciences) followed by permeabilization with ice-cold Perm Buffer III (PBS containing 90% methanol, BD Biosciences) and staining with antibodies for phospho-proteins (listed in Table 2) for 30 minutes at room temperature. Samples were acquired on a LSR II flow cytometer (BD Biosciences) and analysed using FlowJo software

	(TreeStar).
Instrument	LSR Fortessa X20 (5-laser), Amnis imageStreamX Mk2
Software	Flow cytometry Collection: BD FACSDiva v8.0.3 Analysis: FlowJo v10.5.3 Imaging cytometry Collection: INSPIRE Analysis: IDEAS v6.2
Cell population abundance	Post-sort purity was ascertained by running a small aliquot through a cytometer immediately post-sort. Purity was in excess of 99% for all populations assayed.
Gating strategy	The human gating strategy is outlined in Extended data 1. Lymphocytes were pre-gated based on FSC and SSC characteristics. Doublets were excluded based on FSC-A vs FSC-H. Dead cells were excluded based on a live/dead dye. T cells were gated based on TCRa/b, excluding CD1d tetramer positive iNKT cells. Gated T cells were sub-divided based on CD4 and CD8 and subsequently gated on CD45RA and CD27, or CD27 and CD28. The mouse gating strategy is outlined in Extended data 7. Gating was the same as in human samples, with the addition of a bona fide NK cell exclusion using NK1.1 before gating on TCRb and CD1d tetramer. Gates are based on FMO controls.

☒ Tick this box to confirm that a figure exemplifying the gating strategy is provided in the Supplementary Information.